University of Lund

Faculty of Natural Sciences

Institute of Physics

Division of Particle and Nuclear Physics

Measurement of forward-backwards (anti)baryon correlations in proton-proton collisions as a function of multiplicity with ALICE at LHC-CERN

LUNDS UNIVERSITET

Supervisor: Prof. Peter Christiansen
Author: Noel Vincze
Physics MSc

LUND, 2024

Table of Contents

Abstract

Two-particle angular correlations were measured in proton-proton collisions for pions π, kaons K and protons p. The meson results show the expected peak predicted by theory. However the proton results (for baryon-baryon and antibaryon-antibaryon pairs) an anti-correlation is observed. This observation is rooted in the baryon formation after the collision.

Popular Abstract

My thesis is about how protons behave when they collide with each other. The proton is a subatomic particle, but it is not a fundamental particle like the electron is. The proton is made out of smaller, more fundamental particles called quarks. Due to this composition of protons, we are interested in how the fundamental collision between quarks works, and in the collision between protons. Another important thing that we can learn from the collisions is a fifth state of matter called quark-gluon plasma. The first four states of matter are solid, liquid, gas, and plasma. Plasma, essentially is nothing more than a scorching hot, ionised gas. We can find this state of matter in, for instance, stars like our Sun, or in fusion reactors.

The fifth state of matter, quark-gluon plasma which, for short, is QGP, is even hotter than 'normal' plasma, it is so hot that even the nucleons break into its more fundamental components which, are quarks and gluons, hence the name. The interesting thing about QGP is that it is the only environment where we can observe free quarks. The interaction between quarks is the strong force, this force is responsible for keeping the protons, neutrons and nuclei together at lower temperatures. So it is important to study this substance because this is our best way to learn about the dynamics of quarks and gluons.

To sum up there are two main reasons why I am interested in studying proton-proton collision. The first one is that we can learn more about the proton-proton collision, and the second one is that during our study of proton-proton collision, we can master a deeper understanding of the Quark-Gluon Plasma.

Ismeretterjesztő összefoglaló

A szakdolgozat témája a protonok viselkedése az egymással való ütközéseik során. A proton szubatomi részecske, azoban nem elemi részecske, úgymint az elektron. A protont kisebb elemi részecskék alkotják, amelyeket kvarkoknak nevezünk. Az összetételnek köszönhetően érdekel minket, hogy hogyan működnek a kvarkok és a protonok közötti ütközések. A másik fontos dolog, amit ezekből az ütközésekből megtudhatunk, az anyag ötödik halmazállapotára vonatkozik, amelyet kvark-gluon plazmának nevezünk. Az anyag első négy halmazállapota lehet szilárd, folyékony, légnemű és plazmaállapot. A plazma nem más, mint igen magas hőmérsékletű, ionizált gáz. Ez a halmazállapot megtalálható a csillagokban, mint például a Nap, valamint a fúziós reaktorokban is.

Az ötödik halmazállapot, a kvark-gluon plazma (quark-gluon plasma, QGP) még magasabb hőmérsékletű, mint a „hagyományos" plazma. Annyira magas hőmérsékletű, hogy az atommagok is az alkotóelemeikre bomlanak, amelyek nem mások, mint a kvarkok és a gluonok, innen ered a halmazállapot neve. Egy érdekes tény a kvark-gluon plazmával kapcsolatban, hogy ez az egyetlen környezet, amelyben a szabad kvarkok megfigyelhetőek. A kvarkok közötti kölcsönhatás, egy erős nukleáris kölcsönhatás. Ez a kölcsönhatás felelős azért, hogy alacsony hőmérsékleten a protonokat, a neutronokat és az atommagokat egyben tartsa. Ennek a halmazállapotnak a tanulmányozása hozzájárul a kvarkok és a gluonok dinamikájának jobb megértéséhez.

Összegezve: a proton-proton ütközés két okból érdekel minket, az első az, hogy így a proton-proton ütközésről többet tudhatunk meg, és a második az, hogy a proton-proton ütközés tanulmányozása során, a kvark-gluon plazma jellegzetességeit jobban megérthetjük.

La reseña de divulgación

El tema de mi tesis es el comportamiento de dos protones cuando chocan el uno con el otro. El protón es una partícula subatómica, pero no es una partícula fundamental, como sí lo es el electrón. El protón está formado por partículas elementales llamadas quarks. Debido a ésta composición, la colisión entre protones es interesante. En concreto, nos interesa cómo se produce la colisión entre los quarks de los protones. Otra cosa interesnte sobre la que aprender de ésta colisión es el quinto estado de la materia, el llamado plasma de quarks-gluones. El plasma (a secas) es un gas tórrido e ionizado. Podemos encontrar este estado en estrellas como nuestro Sol, o en los reactores de fusión.

Volviendo al quinto estado de la materia plasma de quarks-gluones (PQG) es aún más caliente que el plasma normal. Es tan caliente, que los nucleones se fragmentan es sus partículas elementales, es decir, sus quarks y gluones, de ahí el nombre. Lo interesante del PQG es que es el único ambiente donde se han observado a los quarks libres. La interacción entre los quarks es la fuerza fuerte, la cual es responsable de mantener juntos los protones, los neutrones y el núcleo a una tempertura más baja. Es importante estudiar ésta materia porque es la mejor manera de aprender sobre la dinámica de los quarks y gluones.

En resumen, hay dos razones principales por las que estoy interesado en estudiar la colisión protón-protón. La primera es que podemos aprender más sobre la colisión protón-protón y la segunda es que durante nuestro estudio de la colisión protón-protón, podemos profundizar nuestra comprensión del plasma de quarks y gluones.

Популярная аннотация

В диссертации речь идет о том, как ведут себя протоны которые сталкиваются друг с другом. Протон — субатомная частица, но не такая фундаментальная, как электрон. Протон состоит из меньших и фундаментальных частиц, называемых кварками. Имено из-за такого состава протонов нас интересует, как происходит фундаментальное столкновение между кварками и столкновение между протонами. Еще один важный факт, которий мы можем узнать из столкновений, это пятое состояние материи, называемое кварк-глюонной плазмой. Первые четыре состояния материи — твердое, жидкое, газообразное и плазма. Плазма это не что иное, как раскаленный ионизированный газ. Это состояние материи находится например в звездах, как наше Солнце, или в термоядерных реакторах.

Пятое состояние материи, кварк-глюонная плазма, сокращенно называемая КГП, даже горячее, чем «обычная» плазма, она настолько горячая, что даже нуклоны разлагаются на свои более фундаментальные компоненты, кварки и глюоны, отсюда и название. Самое интересное в КГП то, что это единственная среда, где могут наблюдаться свободные кварки. Взаимодействие между кварками является сильной силой, которая ответсвенна за удержание протонов, нейтронов и ядер вместе при более низких температурах. Это вещество важно изучать, потому что это лучший метод узнать о динамике кварков и глюонов.

Подводя итоги можно сказать, что есть две основные причины, в которых я заинтересован в изучении протон-протонных столкновений. Во-первых, возможно больше узнать о протон-протонном столкновении и понять причину такого явления, а во-вторых, во время изучения протон-протонного столкновения предоставляется возможность глубже понять кварк-глюонную структуру.

抽象的

この卒論文は、陽子が互いに衝突したときにどのように振る舞うかについて書いてある。 陽子は素粒子ですが、電子のような基本粒子ではない。 陽子は、クォークと呼ばれて、より小さく、より基本的な粒子から作られている。 陽子のこの組成により、私たちはクォーク間の基本的な衝突がどのように機能されているか、そして陽子間の衝突に興味を持っている。衝突から学べるもう 1 つの重要なことは、クォーク グルーオン プラズマと呼ばれた物質の 5 番目の状態である。 物質の最初の 4 つの状態は、固体、液体、気体、プラズマである。プラズマは本質的には灼熱のイオン化したガスにすぎない。 この物質の状態は、たとえば、太陽のような星や核融合炉で見つけることができない。

物質の 5 番目の状態であるクォーク グルーオン プラズマ (略して QGP) は、「通常の」プラズマよりもさらに高温であり、非常に高温のため、核子でさえクォークとグルーオンであるそのより基本的な構成要素に破壊される。 QGP の興味深い点は、自由クォークを観察できる唯一の環境であるということである。 クォーク間の相互作用は強い力であり、この力は陽子、中性子、原子核を低温で一緒に保つ役割を果たす。 この物質を研究することが重要である。これは、クォークとグルーオンの力学について学ぶ最良の方法のである。

要約すると、私が陽子間衝突の研究に興味を持っている主な理由は 2 つがある。 1 つ目は、陽子と陽子の衝突についてさらに詳しく学び、その現れる理由を知ることができる。2 つ目は、陽子と陽子の衝突の研究中に、クォーク・グルーオンについてより深く理解できること。

الخلاصة

تدور رسالتي حول كيفية تصرف البروتونات عندما تصطدم ببعضها البعض. البروتون هو جسيم دون ذري، لكنه ليس جسيماًا أساسياًا مثل الإلكترون. يتكون البروتون من جسيمات أصغر وأكثر أساسية تسمى الكواركات. وبسبب هذا التركيب للبروتونات، نحن مهتمون بكيفية عمل التصادم الأساسي بين الكواركات، وفي التصادم بين البروتونات. شيء آخر مهم يمكن أن نتعلمه من الاصطدامات هو الحالة الخامسة للمادة التي تسمى بلازما كوارك-غلوون. الحالات الأربع الأولى للمادة هي الصلبة والسائلة والغازية والبلازما. البلازما، في الأساس، ليست أكثر من غاز متأين ساخن وحارق. يمكننا أن نجد هذه الحالة من المادة، على سبيل المثال، في النجوم مثل شمسنا، أو في مفاعلات الاندماج النووي.

الحالة من المادة، على سبيل المثال، في النجوم مثل شمسنا، أو في مفاعلات الاندماج النووي. الحالة الخامسة للمادة، بلازما كوارك-غلوون والتي للاختصار هي QGP، هي أكثر سخونة من البلازما العادية، فهي ساخنة جداً لدرجة أنه حتى النيوكليونات تنقسم إلى مكوناتها الأساسية، وهي الكواركات والجلونات، ومن هنا يأتي اسمها. الشيء المثير للاهتمام في QGP هو أنها البيئة الوحيدة التي يمكننا من خلالها مراقبة الكواركات الحرة. التفاعل بين الكواركات هو القوة الشديدة، هذه القوة هي المسؤولة عن إبقاء البروتونات والنيوترونات والنوى معاًا في درجات حرارة منخفضة. لذا من المهم دراسة هذه المادة لأنها أفضل طريقة للتعرف على ديناميكيات الكواركات والجلونات.

باختصار، هناك سببان رئيسيان وراء اهتمامي بدراسة تصادم البروتونات. الأول هو أنه يمكننا معرفة المزيد عن اصطدام البروتون بالبروتون ومعرفة سبب ظهور هذا الانخفاض، والثاني هو أنه خلال دراستنا لاصطدام البروتون بالبروتون، يمكننا إتقان فهم أعمق للكوارك-جلوون بلازما.

Introduction

The Standard Model of Particle Physics is the most successful theory in science, which is capable of describing the foundation of almost the entire Universe. The Standard Model (SM) not only describes the fundamental particles but also the three interactions as well. These particles can be grouped into several categories. The main ones are as follows: bosons, particles with integer spin, are the force carriers of the respective interaction and the other type of particles are fermions, particles with half-integer spin. Fermions can be divided into further groups namely quarks and leptons. Leptons are sensitive to the electromagnetic force and the weak interaction. Quarks are sensitive to the strong interaction as well. The strong interaction imposes an interesting condition on the quarks. This condition is that quarks cannot be observed alone but need to form some 'colour-neutral' compound particles. The most common forms, in Nature, of these compound particles are protons and neutrons. These particles, especially protons, play an important role in heavy-ion physics.

Heavy-Ion physics was first started by theoretical physicists Enrico Fermi and Lev Landau in the previous century. These early explorations of hadron matter and multiparticle production paved the way for the thermal description of multiparticle production in the 1960s. Later on, these developments eventually led to the discovery of the quark-gluon plasma. The goal of heavy-ion physics or high-energy nuclear physics is to study the behaviour of heavy-ion collisions, and nuclear matter in high-energies, especially to study quark matter and the strong interaction between quarks. The theory that describes the strong interaction is not easily solvable with perturbation theory. That is why several other approaches have been worked out to make measurable predictions for the quark matter. Perhaps one of the most successful of these approaches is the Lattice Quantum Chromodynamics (Lattice QCD). There are many important applications of Lattice QCD to the study of quark matter. Another important model in the study of quark matter is the Lund string model. The Lund string model is a phenomenological model which is derived from lattice QCD. Essentially this model describes mesons as strongly coupled

dipoles. When these dipoles get separated they undergo the so-called yo-yo effect. Contrary to electromagnetic dipoles when they break apart instead of having two individual quarks, as seen in the electromagnetic case, they form two narrow tubes of strong colour field, also called a string.

Observing or rather measuring these interesting states of matter is not easy. It was proposed that in Nature we could look at neutron stars to study both the hadron and the quark matter however it has not been definitively proven. We need 'on-hand' experiments, that is why we have built the Relativistic Heavy-Ion Collider (RHIC) [22] in the US at the Brookhaven National Laboratory [23] and the Large Hadron Collider (LHC) [25] in Europe at CERN (Conseil Européen pour la Recherche Nucléaire) [24]. The ALICE (A Large Ion Collider Experiment) [7, 28] detector at the LHC at CERN specialises in studying Pb–Pb nuclei collisions, p-Pb nucleus collisions and p-p collisions. The other LHC detectors such as ATLAS (A Toroidal LHC Apparatus) [29], CMS (Compact Muon Solenoid) [27] and LHCb (Large Hadron Collider beauty) [26] all participate in the heavy-ion programme.

Aim and Motivation of the Thesis

The aim of this thesis is the measurement of two-particle correlation between different pseudorapidity regions in proton-proton collisions, using data from the ALICE detector.

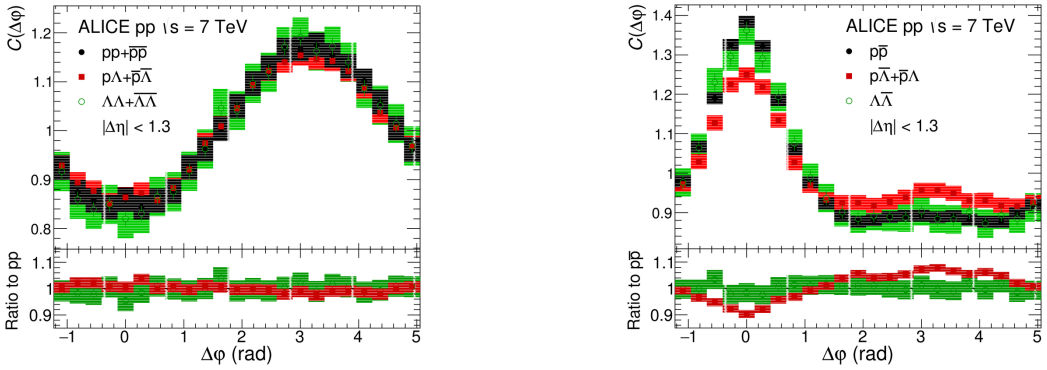

(a) Same baryon correlation

(b) Opposite baryon correlations

Рис. 1: The suppression in the same baryon correlation function as was reported in [1]

The motivation for this thesis comes from the results in [1]. In that paper, they have reported that they have observed suppression in the baryon-baryon and baryon-antibaryon correlation function. The baryons they have looked at were the protons p and lambdas Λ. However, when they looked at the mixed baryon correlation function (p - Λ) they have not observed this depression.

Chapter 1

The Standard Model of Fundamental Particles

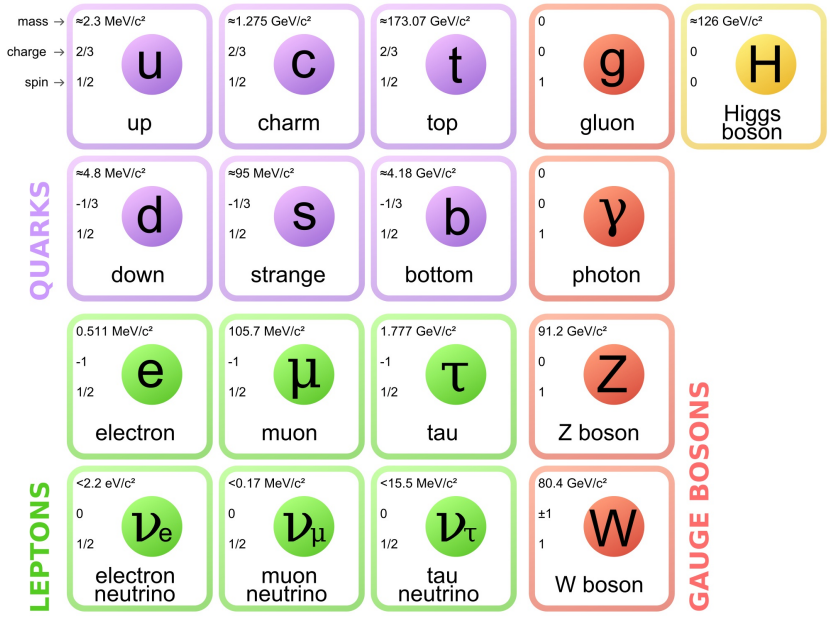

Figure 1.1: The Standard Model of Fundamental Particles and Interactions from [13]. In the first column, we have the first generation of particles, in the second column we have the second generation and finally, in the third column we have the third generation of particles.

The Standard Model of Particle Physics was mainly developed throughout the latter half of the 20th century starting in the 1930s with the Dirac equation, in the 1940s Yukawa's theory of the mesons, then in 1950s with the weak interaction, in the 1960s with Gell-Mann's introduction of the quark model and in the same decade Higgs's description of the spontaneous symmetry breaking, up to the 1970s when Glashow, Weinberg and Salam have introduced the electroweak theory. Throughout the 20th century, many more scientists have contributed to the creation of the Standard Model.

1.1 Fundamental Particles and Forces in The Standard Model

Of the four fundamental forces, the Standard Model describes three of them. They are: the electromagnetic force, the weak force and the strong force. Later on, the electromagnetic and weak interactions have been unified into one force called the electroweak interaction. From the theory perspective, there is hope that these three forces can be combined into one force called the Grand Unified Theory (for further details see [2–5]), however experimentally it remains to be seen if it is true.

The electromagnetic interaction is described by Quantum Electrodynamics (QED), and its Lagrangian is the following

$$\mathcal{L}_{QED} = -\frac{1}{4\mu_0} F^{\mu\nu} F_{\mu\nu} + \bar{\psi}(ic\hbar\gamma^{\mu} D_{\mu} - mc^2)\psi \tag{1.1}$$

Quantum Electrodynamics deals with particles that have electric charge. From this Lagrangian we can obtain two important equations, the Dirac equation for electrically charged fermions and Maxwell's equations which describes the force carrier bosons of the theory, the photons. The matter particles that mainly described by QED are leptons, and they have a spin of $\frac{1}{2}$ and the electric charge of ± 1. The particles that belong to the leptons are the electron, muon, tau and their neutrino counterparts. The generations of leptons (see Fig. 1.1) are as follows: electron and its neutrino (1st generation), muon and its neutrino (2nd generation), tau and its neutrino (3rd generation). The photon has a spin of 1, is electrically neutral and is a vector boson.

The strong interaction is described by Quantum Chromodynamics (QCD), and its Lagrangian is the following

$$\mathcal{L}_{QCD} = \sum_{n=1}^{6} \bar{\psi}_n (ic\hbar\gamma^{\mu} D_{\mu} - m_n c^2)\psi_n - \frac{1}{4} G^a_{\mu\nu} G^{\mu\nu}_a \tag{1.2}$$

In the strong interaction, the participating particles are the quarks, from which we have six (see Fig. 1.1) namely up and down (1st generation), charm and strange (2nd generation), top and bottom (3rd generation). Quarks have a spin of $\frac{1}{2}$ and the electric charge of $+\frac{2}{3}$ or $-\frac{1}{3}$, and they have the additional property called the colour charge. The colour charge is the charge of the strong interaction and can take the following values: red, green, and blue. It is inspired by the colour combination of optics but it is best not to read too much into it. The gluons are the force carriers of the theory and in contrast to QED we have eight of them and they are capable of interacting with each other. The gluons have a spin of 1, electrically neutral and they have 8 linearly independent combinations of colour and anti-colour charge and they are a vector bosons. The strong force is also responsible for creating composite particles. We categorize them as mesons or baryons. The important constructing principle is that the colour combination of the composite particle is white or neutral so that the particle would have no colour charge in the end. Mesons are constructed from two quarks (one with a colour charge and the other with the opposite colour charge), more specifically from a quark and an anti-quark. Baryons are constructed from three or more quarks. Each baryon also has an anti-particle called the anti-baryon, constructed from anti-quarks.

The weak interaction is responsible for the radioactive decay of atoms. It is described by the GSW theory and its Lagrangian is

$$\mathcal{L}_{GWS} = \mathcal{L}_{Maxwell} + \mathcal{L}_{fermion} + \mathcal{L}_{Higgs} \tag{1.3}$$

where these Lagrangians mean the following

$$\mathcal{L}_{Maxwell} = -\frac{1}{4\mu_0}(F_{\mu\nu})^2 \tag{1.4}$$

$$\mathcal{L}_{fermion} = i\bar{\psi}_L\gamma^\mu D_\mu\psi_L + i\bar{\psi}_R\gamma^\mu D_\mu\psi_R \tag{1.5}$$

$$\mathcal{L}_{Higgs} = |D_\mu\phi|^2 + \mu^2|\phi|^2 - \frac{\lambda}{2}(|\phi|^2)^2 \tag{1.6}$$

The terms in the GSW Lagrangian are the following: The Maxwell term describes the electromagnetic boson, the fermion term describes the fermions such as electron, muon, tau and their neutrinos, the subscripts of L and R refer to the left or right-handedness of the particle, and the Higgs term is responsible for the symmetry breaking. Weak interaction is special in the sense that it violates CP symmetry (Charge-Parity symmetry) when it comes to neutrinos. That is, nature distinguishes between left and right-handed neutrinos.

1.2 The Asymptotic freedom and the Jet quenching

The strong interaction is said to be asymptotically free meaning that the more we separate two quarks the stronger the strong force grows between them. Hadrons are formed from quarks that are in close proximity to each other and are bound by gluon exchange.

When we finally separate the two quarks far enough from each other, instead of breaking and giving us two individual quarks (as is the case for an electric dipole) those quarks going to be formed into mesons so that the principle of colour neutrality would be respected. This is also why we say that the quarks are confined into hadrons.

When two beams of accelerated hadrons collide they create the fifth state of matter called the Quark-Gluon Plasma (QGP). These particles that participate in the collision called partons, traverse the medium of QGP and then they either form an isotropic 'ball' or they form jets. Jets typically form back-to-back, however, experiments in heavy ion physics show that this is not the case for particles that participate in the strong interaction. The suppression of jets is also called jet quenching. But what is quenching? Quenching, in general, is defined as the rapid cooling by immersion in oil/water, of a metal object from the high temperature at which it has been shaped. In particle physics jet quenching means that the opposite jet is reduced because of the interaction with QGP medium suppress it.

Chapter 2

High-Energy Physics

High-energy physics is the study of the most fundamental particles in our Universe. It is interesting because we can literary study the building blocks of our Universe. Furthermore, it allows us to discover the inner workings of Nature.

2.1 Experimental variables of Particle physics

To be able to discuss the results in the upcoming sections we need to clarify some basic concepts regarding experimental particle physics. First of all, we are going to discuss quantities like the transverse momentum, energy and mass. The transverse momentum is defined as

$$p_T = \sqrt{p_x^2 + p_y^2} \tag{2.1}$$

This transverse momentum is the component in the momentum $\mathbf{p}$ which is perpendicular to the beamline (the beam line typically is in the z direction).

The momentum along the beam is also called the longitudinal momentum p_L but in most cases, it will be simply denoted as p_z. The transverse mass is defined by the following equation

$$m_T = \sqrt{p_T^2 + m^2} \tag{2.2}$$

Finally the transverse energy is defined as

$$E_T = \frac{E}{\cosh(y)} \tag{2.3}$$

where y is the rapidity. The magnitude of the three-momentum read

$$|\mathbf{p}| = p_T \cosh(y) \tag{2.4}$$

Thus the components of the four-momentum p^μ in terms of transverse momentum p_T read

$$p^0 = \frac{E_T}{c}\,\cosh(y) \tag{2.5}$$

$$p^1 = p_T\,\cos(\phi) \tag{2.6}$$

$$p^2 = p_T\,\sin(\phi) \tag{2.7}$$

$$p^3 = p_T\,\sinh(y) \tag{2.8}$$

Nowadays the most common way to express the Lorentz transformation is with the relative velocity $\boldsymbol{\beta}$, which is defined as $\mathbf{v}$/c. Historically H. Minkowski expressed this transformation with hyperbolic sine and cosine of a quantity called rapidity y. The Lorentz factor in terms of rapidity reads

$$\gamma = \frac{1}{\sqrt{1-\boldsymbol{\beta}^2}} = \cosh(y) \tag{2.9}$$

Using the mass-energy relation and the Lorentz transformed energy and momentum we find for rapidity:

$$y = \frac{1}{2}\ln\left(\frac{E+p_z c}{E-p_z c}\right) \tag{2.10}$$

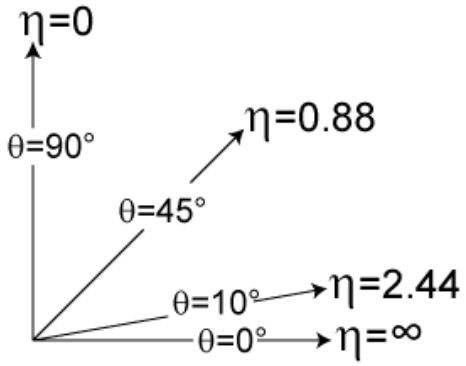

Figure 2.1: Pseudorapidity values shown on a polar plot. An angle of zero is usually along the beam axis, and thus particles with high pseudorapidity values are generally lost, escaping through the detector along with the beam. As polar angle approaches zero, pseudorapidity tends towards infinity. Image from Ref. [12]

Another quantity that is useful to us in experimental physics, in particular for unidentified particles is called pseudorapidity. It is defined as

$$\eta = -\ln\left(\tan\left(\frac{\theta}{2}\right)\right) \tag{2.11}$$

where θ is the angle between the particle three-momentum $\mathbf{p}$ and the positive direction of the beam axis. In the limit when $m \ll p_T$, the particle energy E is approximately equal to the magnitude of the three-momentum $|\mathbf{p}|$ and thus pseudorapidity η converges to rapidity y. This limit of pseudorapidity changing into rapidity can be seen much clearer from another expression for pseudorapidity η, which reads

$$\eta = \frac{1}{2}\ln\left(\frac{|\mathbf{p}|c + p_z c}{|\mathbf{p}|c - p_z c}\right) \tag{2.12}$$

which can be compared with the definition of y, that is with Eq.2.10.

A final quantity that we need to talk about is the centre of mass energy. It is defined as

$$E_{cm} = \sqrt{\left(\sum_i E_i\right)^2 - \left(\sum_i \mathbf{p}_i\right)^2} \tag{2.13}$$

The centre of mass energy is most commonly denoted not by E_{cm} but by $\sqrt{s}$. The s comes from Quantum Field Theory (QFT for short), where it is one of the Mandelstam variables, and signifies the centre of mass energy squared. In Heavy ion collision, we can see the quantity $\sqrt{s_{NN}}$ which denotes that we are dealing with several more constituents in the collision between nuclei. In the center of mass the total momentum $\sum_i \mathbf{p}_i = 0$ thus $\sqrt{s}$ will give us the energy at which the collision happens. For a more hands-on understanding of the basics see Ref. [18].

2.2 Quark-Gluon Plasma

In high-energy collisions the fifth state of matter is formed, called the Quark-Gluon Plasma (QGP). In the QGP quarks and gluons asymptotically roam free. However this state of matter can only be created with high temperatures and/or pressures, and in Nature, they only occurred after The Big Bang and possibly in heavy neutron stars. If we desire to study this state of matter experimentally then we need to build powerful accelerators that can make head-on collisions between heavy ions. These powerful accelerators are the Relativistic Heavy Ion Collider (RHIC) and the Large Hadron Collider (LHC). A Large Ion Collider Experiment (ALICE) is an experiment that specialises in the study of heavy-ion collisions. In

these experiments, the typical ions we use are gold (Au) and lead (Pb) but we also study proton-proton collisions. In the fireball created by the collision of heavy ions, quarks and gluons are free for a brief amount of time and afterwards, the QGP cools down and the partons recombine into ordinary hadrons. These processes are fundamental to the research into Quantum Chromodynamics (QCD) and to the description of the strong force. An interesting property of the QGP that it behaves more similar to a perfect fluid with a small amount of viscosity rather than a very hot gas.

2.3 PYTHIA

PYTHIA (for details see [15]) is a Monte Carlo (MC for short) event generator that is specialised for the description of hadrons. It generates collisional events that mimic the real data. To make it better suited to describe the real data set, new parameters are introduced that represent quantum mechanical randomness. PYTHIA simulations resemble the real data however the best way to use it is to compare it with real data. To simulate the collisional events it uses the Lund String model.

2.4 The Lund String Model

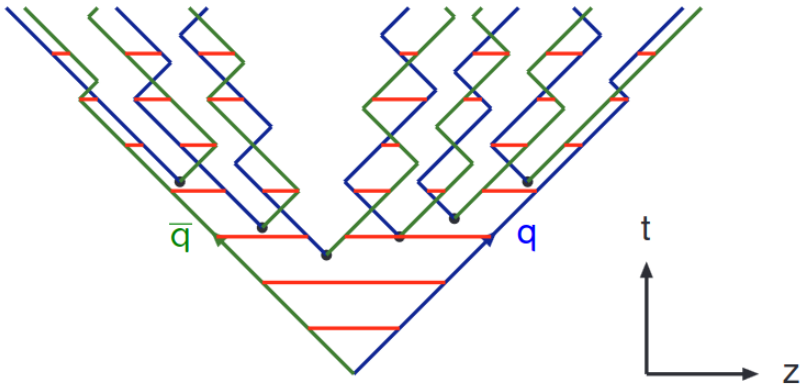

Figure 2.2: The motion of quarks and anti-quarks. This image shows why their motion is referred to as yo-yo motion. Image from [14]

The Lund String Model (see [14, 15]) is derived from the results in lattice QCD which supports the view that the force interacting between two colour-charged particles is so strong that it can be modelled as a flux tube where the energy increases linearly with the distance between two colour charged particle (like $q\bar{q}$ pair). As the particles move apart the energy gets transferred from the particles to the string itself creating the so-called "yo-yo" effect. Essentially the potential of a colour-charged dipole can be simply modelled as a spring which has the potential of $V(r) \approx k\,r$ where k is the spring/string constant. In the this interpretation, like the dipole's yo-yo model, corresponds to a meson with the flavour determined by the quark content of the string. Longer strings will break into smaller strings and eventually form hadrons. This process is called hadronization.

Chapter 3

Particle Identification

An important aspect of particle physics is to be able to identify particles and map their properties. In order to identify them we use different methods. Common methods include measuring the energy loss of particles by ionisation and time of flight.

3.1 Measurement of Momentum in a magnetic field

The Lorentz force in relativistic four-vector notation, says

$$\frac{dp^{\mu}}{d\tau} = eF^{\mu}{}_{\nu}\, u^{\nu} \tag{3.1}$$

where $F^{\mu}{}_{\nu}$ is the field strength tensor for the electromagnetic field and e is the electric charge. If we break this equation into the usual three-vector notation we have

$$\frac{dE}{dt} = eE^{j}u_{j} \tag{3.2}$$

$$\frac{dp^{i}}{dt} = e\left(E^{i} + \varepsilon^{ijk}u_{j}B_{k}\right) \tag{3.3}$$

where the first line describes the particle's energy, the particle loses energy due to the electric field, and in the second line, we have the usual Lorentz force in

three-vector notation. In the lab frame of reference, the equation reduces to

$$\frac{dE}{dt} = 0 \tag{3.4}$$

$$\frac{dp^i}{dt} = e\,\varepsilon^{ijk} u_j B_k \tag{3.5}$$

The Lorentz force is used to measure the momentum of a track. In these detectors, we typically have a magnetic field $\mathbf{B}$ in the z direction only, which coincides with the beam direction, hence we can measure the particle's transverse momentum. Then the Lorentz force equation reduces to

$$\frac{du^i}{dt} = \frac{eB}{m}\,\varepsilon^{ijk} u_j \hat{e}_k = \omega_B \varepsilon^{ijk} u_j \hat{e}_k \tag{3.6}$$

where ω_B is the cyclotron frequency, and $\hat{e}_k = (0, 0, \hat{z})$ is the basis vector. These equations of motion have the solution of a harmonic oscillator in the x and y direction and a free particle in the z direction. We find that p_T is equal to

$$p_T = m\omega_B R \tag{3.7}$$

where R is the radius of the cyclotron motion. Thus allowing us to extract the p_T from measurements of the particle as it moves through the magnetic field.

3.2 Bethe-Bloch Formula

An important tool in identifying particles is the "Bethe-Bloch" plot. The plot can be made only for stable and long-living particles. These particles are the following: electron e, proton p, pion π and kaon K. Pions π and kaons K are not stable particles but rather long-living ones.

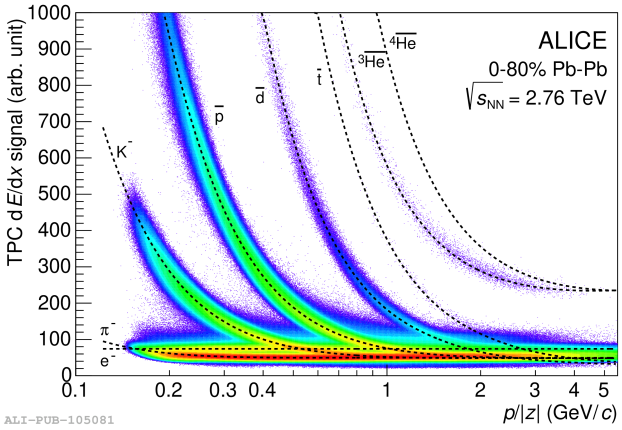

Figure 3.1: The Bethe-Bloch plot from [7]

As we can see on 3.1 we can also see two nuclei (deuterium $\bar{d}$ and tritium $\bar{t}$) and also two isotopes of Helium (Helium-3 and Helium-4). The Bethe-Bloch formula describes the energy loss of a charged particle moving through a medium. For a general material, the equation takes the form of

$$-\frac{dE}{dx} = 4\pi n Z_m \frac{Z^2\alpha^2\hbar^2}{m_e\beta^2}\left[\ln\left(\frac{2m_e c^2\gamma^2\beta^2}{I}\right) - \beta^2\right] \tag{3.8}$$

where m_e is the electron's mass, ε_0 is the vacuum permittivity, β is the relative velocity of the particle, n is the density of the electron and I is the ionization potential. The Z_m stands for the charge of the material, and α is the fine structure constant, which has the approximate value of $\alpha \approx 1/137$.

The stopping power dE/dx is independent of the mass of the incoming particle, it depends on the incoming particles' charge Z and, treating the logarithmic term as a constant (it varies slowly compared to the quadratic term), on the relative velocity β as

$$\frac{dE}{dx} \propto \frac{1}{\beta^2} \tag{3.9}$$

There are three interesting limits of the Bethe-Bloch formula. These are the low-velocity regime, the minimum ionisation loss and the relativistic rise.

In *the low-velocity regime* we have $\gamma\beta < 3.5$, which means that slow-moving positively charged particles can capture the detector's electrons, which will reduce the effective charge Z which in turn will reduce stopping power $-dE/dx$. In *the minimum ionisation* we have $\gamma\beta \approx 3.5$, where the γ^2 term in the logarithm decreases

the stopping power. *The relativistic rise* happens when $\gamma\beta > 3.5$, meaning that the Bethe-Bloch formula starts to rise indefinitely. Furthermore, the relativistic particles transverse electric field increases hence increasing the ionisation effect in the material.

3.3 Time Of Flight

The time of flight measurement relies on the TOF detector. In this measurement, we measure the estimated velocity of the particle. The measurement is carried out the following way: there are two detectors separated by a distance L, when a particle traverses the detectors one of them will be triggered indicating the start and the other indicating the stop signal. The time of flight is given by the formula:

$$\Delta t = \frac{L}{c}\sqrt{\frac{p^2 + m^2c^2}{p^2}} \tag{3.10}$$

where L is the distance between the detectors, c is the speed of light, p is the magnitude of the momentum of the particle, and m is the mass of the particle. Expressing the mass from the time of flight we get

$$m^2_{TOF} = \frac{p^2}{c^2}\left(\left[\frac{\Delta t\, c}{L}\right]^2 - 1\right) \tag{3.11}$$

which is called the time of flight mass. Essentially what we do here is Time Of Flight Mass Spectroscopy (TOFMS). The TOF measurements are applied between 0.3 - 4 GeV. This method is useful for the measurement of the production of p, K and π.

Chapter 4

A Large Ion Collider Experiment

A Large Ion Collider Experiment or ALICE for short, is an experiment that is optimized for the study of heavy-ion physics. In order to study the strongly interacting matter ALICE produces extreme densities and temperatures where a new phase of matter is formed called the QGP.

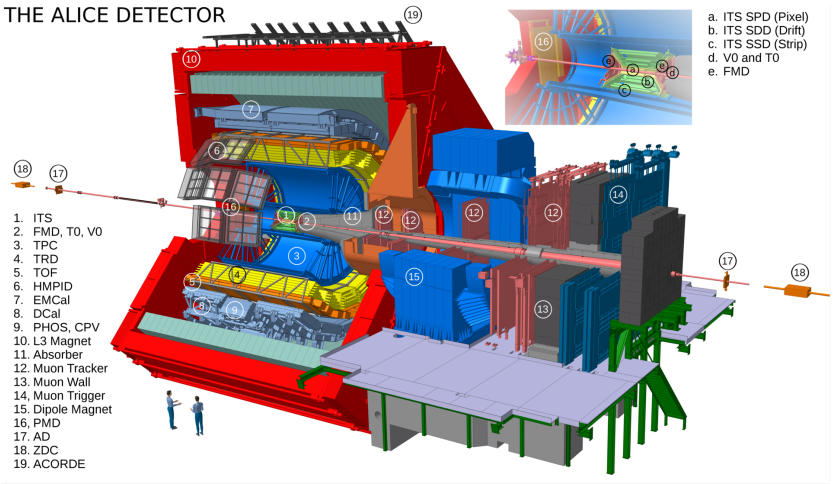

Figure 4.1: The schematical view of the ALICE detector. The detectors used in this thesis are the TOF, the TPC, the SPD, and the Forward Multiplicity Detectors. Image from [7]

4.1 Inner Tracking System

The Inner Tracking System or ITS for short, consists of several layers of silicon detectors, six in total. The job of the ITS is to measure the track position and the energy loss of the particles in the collision. The layers are grouped into pairs, giving us three individual detector systems in total. The innermost two layers are the Silicon Pixel Detector (SPD). The SPD has a continuous coverage of the pseudorapidity η hence gives us a good measurement of the charged-particle multiplicities. The SPD detectors cover the pseudorapidity in the ranges of $-2.0 < \eta < 2.0$ and $-1.4 < \eta < 1.4$ respectively. SPD tracklets are used through out in this thesis and is refered to as CL1. A tracklet is by definition a 2-point track segment between two SPD hits. The CL1 is used to measure the multiplicity of the collision. This multiplicity is given by counting the number of tracklets using the SPD in the pseudorapidity range of $-0.8 < \eta < 0.8$ and gives the estimated multiplicity in the central region of the ALICE detector.

The next two layers are called the Silicon Drift Detector (SDD). These detectors are suitable for reading out energy-loss information which can be used for particle identification. The last two layers are called Silicon Strip Detector (SSD). These detectors measure the position of the track as well as the energy-loss of the particle(s).

4.2 V0

The V0A and V0C are scintillator detectors and they are located on each side of the beam. The V0A covers the pseudorapidity in the range of $2.8 < \eta < 5.1$ while the V0C covers the pseudorapidity in the range of $-3.7 < \eta < -1.7$. The V0 detector is an example of a Forward Multiplicity Detector. In the ALICE we have the V0A and the V0C detector which get combined into V0M by the formula: $V0M = V0A + V0C$. Scintillation is the process when excited materials emit visible or UV light. This process can happen in inorganic crystals, organic liquids and plastics (the latter two are commonly applied in particle physics). A scintillation-based detector or scintillator works that after the scintillation light is emitted it passes down to a photo-multiplier which in the end will give an electrical signal. This electrical signal is then further enhanced which in turn used to count the number of particles that have passed through the detector.

4.3 Time Projection Chamber

The Time Projection Chamber or TPC for short, can be found in the middle part of the ALICE detector. The ALICE TPC detector covers the pseudorapidity in the range of $-0.9 < \eta < 0.9$. The detector is divided into two drift regions by the central electrode located at its axial centre. The TPC is a gas base detector containing a mixture of Ne, CO_2 and N_2. There is a uniform electric field along the z-axis which drifts the electrons to the two end plates of the electrode. The TPC detector works on the principle that charged particles traversing a medium, in this case, the volume of the TPC will ionise the gas along their path, freeing electrons from their atomic bands and then those electrons drift towards the electrode where they create an electric signal. This signal is amplified by Multi-Wire Proportional Chamber which is used for the tracking of charged particles. This was updated to Gas Electron Multipliers recently.

4.4 Time Of Flight

The Time of Flight or TOF for short, can be found in the outer region of the ALICE detector. The ALICE TOF detector covers the pseudorapidity interval of $-0.9 < \eta < 0.9$. The TOF measures the time that each particle takes to travel from the centre of the collision to the detector itself, hence the speed of the particle can be measured. It provides charged particle PID in the intermediate momentum range.

Chapter 5

Analysis

5.1 Two Particle Correlations

Two particle correlations are essential for the study of forward-backwards correlations. For two-particle, where particle i has the pseudorapidity of η_i and particle j has the pseudorapidity of η_j, the correlation function is given by

$$C(\eta_i, \eta_j) = \frac{\langle N(\eta_i)N(\eta_j)\rangle}{\langle N(\eta_i)\rangle\langle N(\eta_j)\rangle} \tag{5.1}$$

where $N(\eta_i)$ is the ith particle multiplicity density distribution and $\langle\rangle$ denote the average for the given event. The two-particle correlation function returns a distribution for the possibility of different particle pairs being created. As any distribution in statistics, the two-particle correlation function (technically a distribution) is normalized to one. In an equation, it says:

$$\langle C(\eta_i, \eta_j)\rangle = 1 \tag{5.2}$$

When the correlation function's value $C(\eta_i, \eta_j)$ is one, it means that the two are on average independent while the correlation function's value $C(\eta_i, \eta_j)$ being less than one corresponding to the two being less correlated while its value being more than one corresponds to the two tracks being more correlated. The multiplicity density distribution $N(\eta_i)$ is very sensitive to the early-time configuration of the system which can also be seen from that correlated particles are the result of these early-time configurations. In the Lund string model, this is interpreted as that correlated particles can be produced only from the same string.

5.2 Same and Mixed events

In the same event (SE) distribution we pick two particles with pseudorapidities η_i and η_j respectively. Hence for an SE, we can make any combination of tracks as long as they were measured in the same event. Same event distributions will be denoted as $S(\eta_i, \eta_j)$ and it is approximately given by

$$S(\eta_i, \eta_j) \propto \langle N(\eta_i) N(\eta_j) \rangle \tag{5.3}$$

On the other hand, in a mixed event (ME) distribution, we pick two particles with pseudorapidities η_i and η_j that are not from the same event. The mixing of particles from different events is used to correct for detector inefficiencies and other non-physical correlation. Mixed event distributions will be denoted as $M(\eta_i, \eta_j)$ and it is approximately given by

$$M(\eta_i, \eta_j) \propto \langle N(\eta_i) \rangle \langle N(\eta_j) \rangle \tag{5.4}$$

Now we are in a place where we can give the two-particle correlation function $C(\eta_i, \eta_j)$ in terms of SE and ME distributions. Hence we have

$$C(\eta_i, \eta_j) = \frac{\langle N(\eta_i) N(\eta_j) \rangle}{\langle N(\eta_i) \rangle \langle N(\eta_j) \rangle} \propto \frac{S(\eta_i, \eta_j)}{M(\eta_i, \eta_j)} \tag{5.5}$$

Particles with similar pseudorapidity $\eta_i \approx \eta_j$, are referred to as short-range correlations while particles with different pseudorapidity $|\eta_i - \eta_j| \gg 0$ are referred to as long-range correlations.

5.3 Selecting events and tracks

For the event selection, first, we impose that the recorded event does not overlap with other events or background events. Secondly, we impose that a primary interaction vertex was successfully reconstructed. The vertices are found by using the SPD detector, i.e., the first two layers of the ITS detector. A vertex is defined as the space point where the maximum number of tracklets originate. Lastly, we need the position of the reconstructed vertices be along the beam line, within 10 cm of the center of the detector.

For the track selection, called ALICE ITSTPC2011, track cuts were employed. The ALICE ITSTPC2011 track cuts are optimized for the best transverse momentum resolution and to avoid contamination from secondary tracks. This was obtained

by demanding that the tracklets in the TPC and in the ITS are matching while at least one SPD hit was recorded for the track. To reject particles that were not directly created during the collision, such as particles originating from interaction with the detector's material or from weak decay processes or from background events, the track was required to point to the vertex (tight cut).

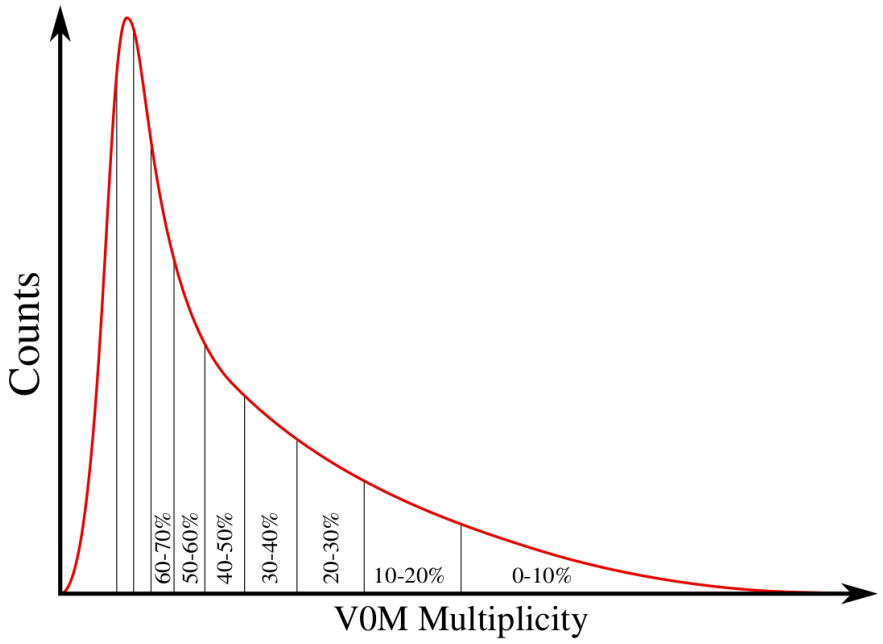

Figure 5.1: Multiplicity classes. [21]

5.4 Multiplicity Classes

The analysis starts with choosing a multiplicity estimator (V0M or CL1) in which we can choose a multiplicity class. The data set was divided into three different multiplicity classes. These are the following: 0-10%, 10-30% and, 30-100%. Then each class had a charge combination (same or opposite) setting, as well as the type of detector (TPC or TOF) could be chosen as well. In general the TPC was used more but for the kaons the TOF was more suitable. Hence all tracks within a given multiplicity interval have been calculated for a given same event or a mixed event distribution.

5.5 Fitting function

To have a better understanding of the 2D plots of the two-particle correlation function $C(\eta_i, \eta_j)$ a fit is implemented. As we can see on 6.1 the pseudorapidities either form a correlation or an anticorrelation. To be able to effectively describe these correlations we define two new variables. These are

$$\eta_+ = \eta_i + \eta_j \tag{5.6}$$

$$\eta_- = \eta_i - \eta_j \tag{5.7}$$

Small values of η_- correspond to short-range correlations while large values of η_- correspond to long-range correlations. The following fitting function was defined and used:

$$F(\eta_+, \eta_-) = f(\eta_+)\, g(\eta_-) + C \tag{5.8}$$

where C is some constant. The function $f(\eta_+)$ is a simple polynomial of degree two given by

$$f(\eta_+) = A\eta_+^2 + C \tag{5.9}$$

where A and C are some constant. The linear term is missing because this function $f(\eta_+)$ must be symmetric. The function $g(\eta_-)$ is a Gaußian with the mean μ is zero. It is given by

$$g(\eta_-) = \frac{1}{\sqrt{2\pi\sigma^2}} \exp\left[-\frac{1}{2}\left(\frac{\eta_-}{\sigma}\right)^2\right] \tag{5.10}$$

where σ is the standard deviation and is a constant. All the constants in the above equations are determined during the fitting process. The fitting function in Eq. 5.8 describes a linear polynomial along the bottom left and the top right with a Gaußian spread along the bottom right and top left.

Chapter 6

Results

In this chapter, the results will be presented. In the first section the general results will be discussed and compared with [21]. In the remaining sections, the PID results will be presented and discussed.

6.1 General

For the reproduction of the results in [21] the LHC18b data set was used. These results will be grouped in the following by multiplicity estimator (V0M and CL1) and within an estimator by charge combination (same and opposite). For the same charge, the following notation is used $++/--$ while for the opposite charge, the notation used is +-/-+ . The results shown in 6.1 are shown with the fitting function $F(\eta_+, \eta_-)$ as a contour plot.

6.1.1 V0M estimator

In this subsection we are presenting the results from the V0M multiplicity estimator.

First of all we are starting with the opposite charge combination. In Fig. 6.1 we can observe a correlation in each multiplicity class. The only difference between the first row and the second row are that the second row has higher statistics thanks to the full LHC18b dataset. We observe a strong positive correlation along the diagonal where two particles are close in pseudorapidity, while the correlation decreases and becomes negative as the difference in pseudorapidity grows.

The new results agree with the results from [21] for the V0M estimator. The fits are plotted the same way as in [21].

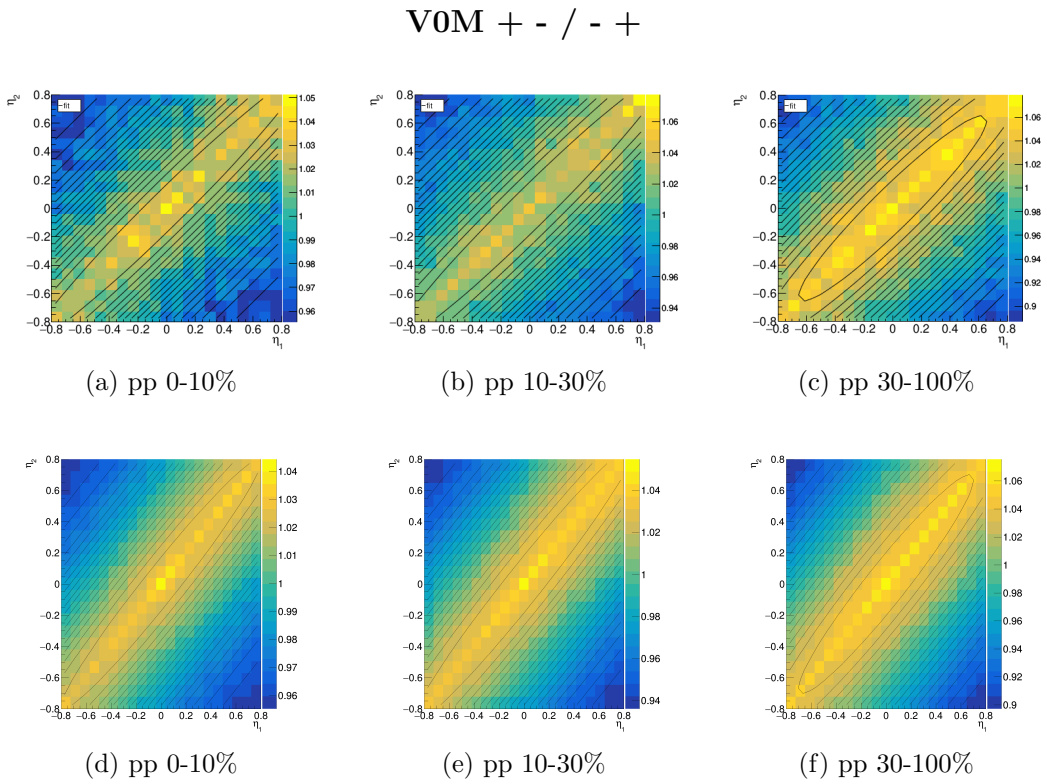

(a) pp 0-10% (b) pp 10-30% (c) pp 30-100%

(d) pp 0-10% (e) pp 10-30% (f) pp 30-100%

Figure 6.1: V0M estimator results for opposite charge combination for different multiplicity classes. In the first row are the results from [21]. In the second row are the new results.

Secondly, we have the same charge combination in Fig. 6.2 We observe a strong positive correlation along the diagonal where two particles are close in pseudorapidity, while the correlation decreases and becomes negative as the difference in pseudorapidity grows.

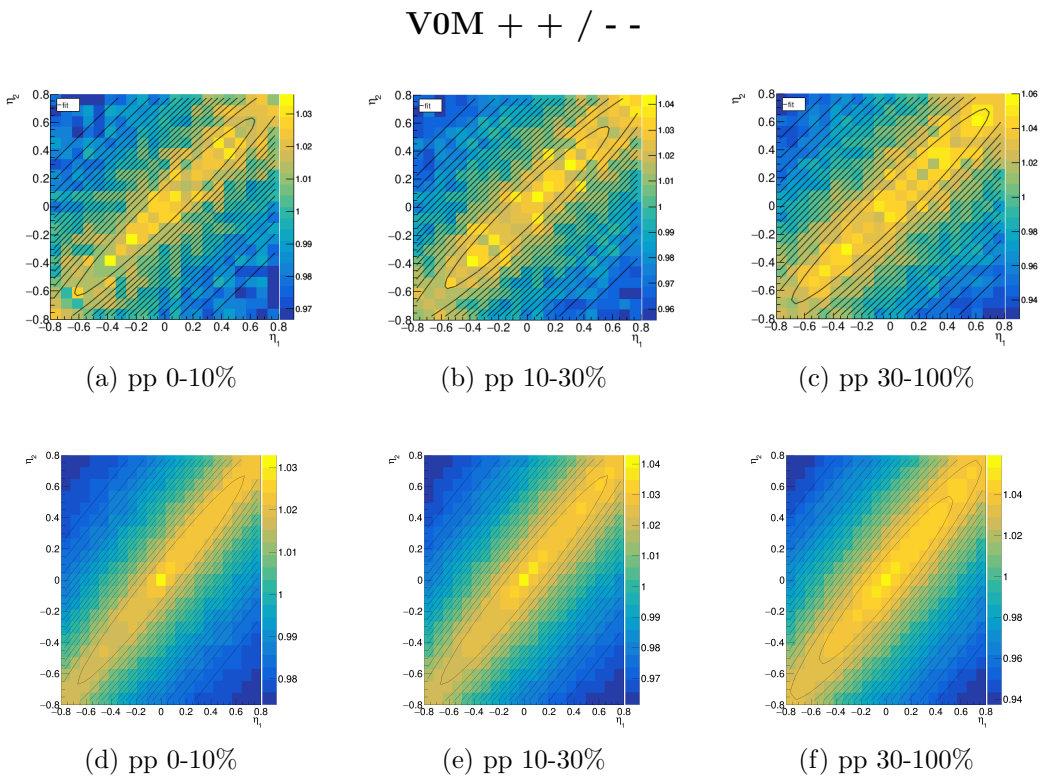

(a) pp 0-10% (b) pp 10-30% (c) pp 30-100%

(d) pp 0-10% (e) pp 10-30% (f) pp 30-100%

Figure 6.2: Same as Fig. 6.1 but for the same charge combination.

In conclusion, the V0M estimator results from [21] and the new results agree. The new results look a promising in the sense that for higher statistics the expected positive correlation does not change.

6.1.2 CL1 estimator

In this subsection, we are presenting the data from the CL1 multiplicity estimator.

First we start with the opposite charge combination. In Fig. 6.3 we observe a correlation in each multiplicity class. There are two main differences between the first and the second row. One of them is that the second row has higher statistics thanks to the full LHC18b dataset, while the other is that 0-10% multiplicity class is different in the second row than in the first. The difference is that in [21] the author divided with mixed event histogram of the V0M multiplicity class instead of the Cl1. We observe a strong positive correlation along the diagonal where the two particles are close in pseudorapidity, while the correlation increases and

becomes negative as the difference in pseudorapidity grows.

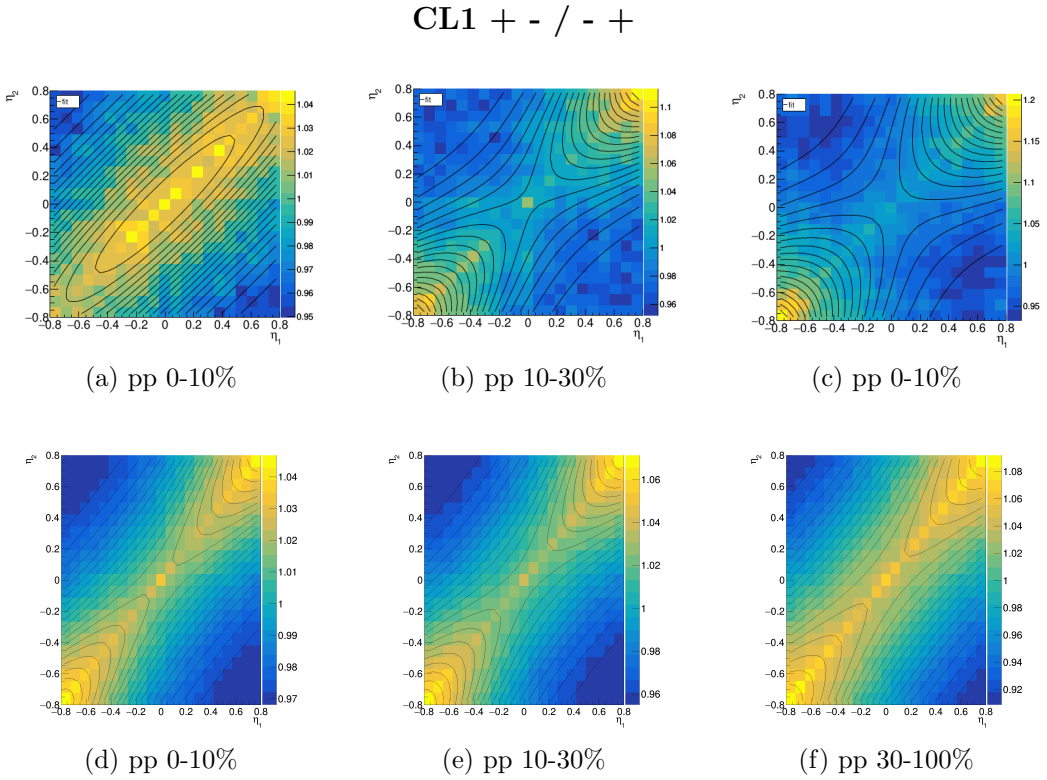

(a) pp 0-10% (b) pp 10-30% (c) pp 0-10%

(d) pp 0-10% (e) pp 10-30% (f) pp 30-100%

Figure 6.3: CL1 estimator results for opposite charge combination for different multiplicity classes. In the first row are the results from [21]. In the second row are the new results.

Secondly, we have the same charge combination. In Fig. 6.4 we can observe a correlation in each multiplicity class. There are two main differences between the first row and the second. One of them is that the second row has higher statistics thanks to the full LHC18b dataset, while the other is that 0-10% multiplicity class is different in the first row than in the second one. The difference comes from that in [21] the author divided with mixed event histogram of the V0M multiplicity class instead of the Cl1. We observe a strong positive correlation along the diagonal where the two particles are close in pseudorapidity, while the correlation increases and becomes negative as the difference in pseudorapidity grows.

In conclusion, the V0M estimator results from [21] and the new results mostly agree. The only difference is observed in the 0-10% multiplicity class. The new

CL1 + + / - -

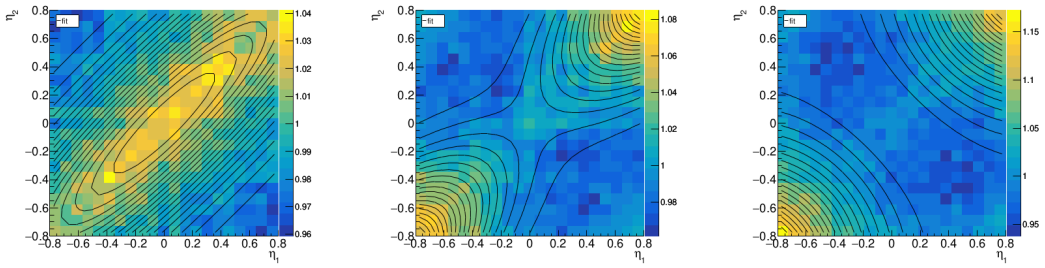

(a) pp 0-10% (b) pp 10-30% (c) pp 30-100%

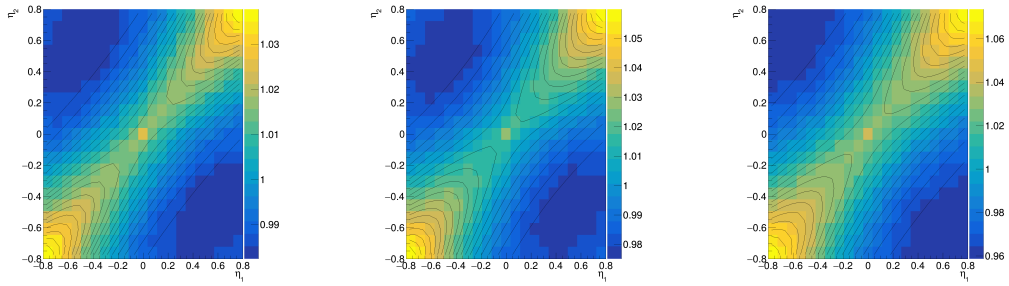

(d) pp 0-10% (e) pp 10-30% (f) pp 30-100%

Figure 6.4: Same as Figure 6.3 but for the same charge combination

results look a promising in the sense that for higher statistics the expected positive correlation does not change.

6.1.3 Same and Opposite charge combination

As in the previous subsections we have seen different charge combinations is an important tool in comparing and understanding the results. What we observe in Figures 6.3,6.4,6.1,6.2 that the opposite charge combination is much more active throughout the multiplicity classes than the same charge combination. This enhancement in activity comes from the fact particle properties are conserved (such as electric charge, baryon number and lepton number).

V0M charge combination comparison

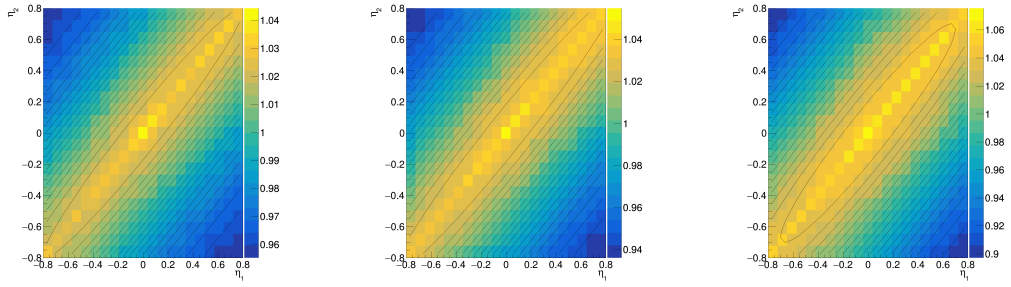

(a) + - / - + 0-10% (b) + - / - + 10-30% (c) + - / - + 30-100%

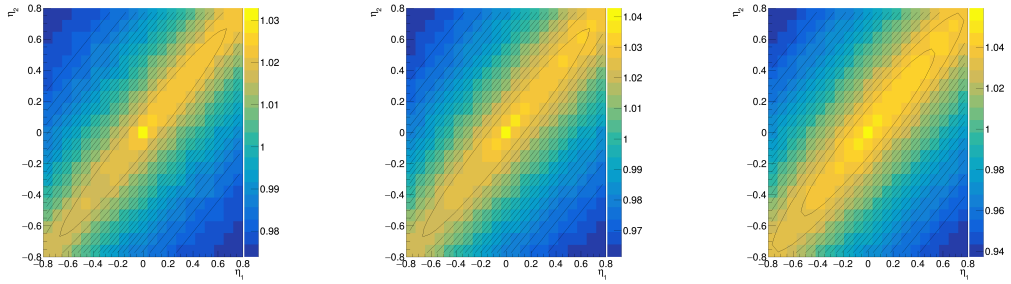

(d) + + / - - 0-10% (e) + + / - - 10-30% (f) + + / - - 30-100%

Figure 6.5: In the first row are the opposite charge combination results, while in the second row are the same charge combination results. In both lines, V0M estimator results are shown.

CL1 charge combination comparison

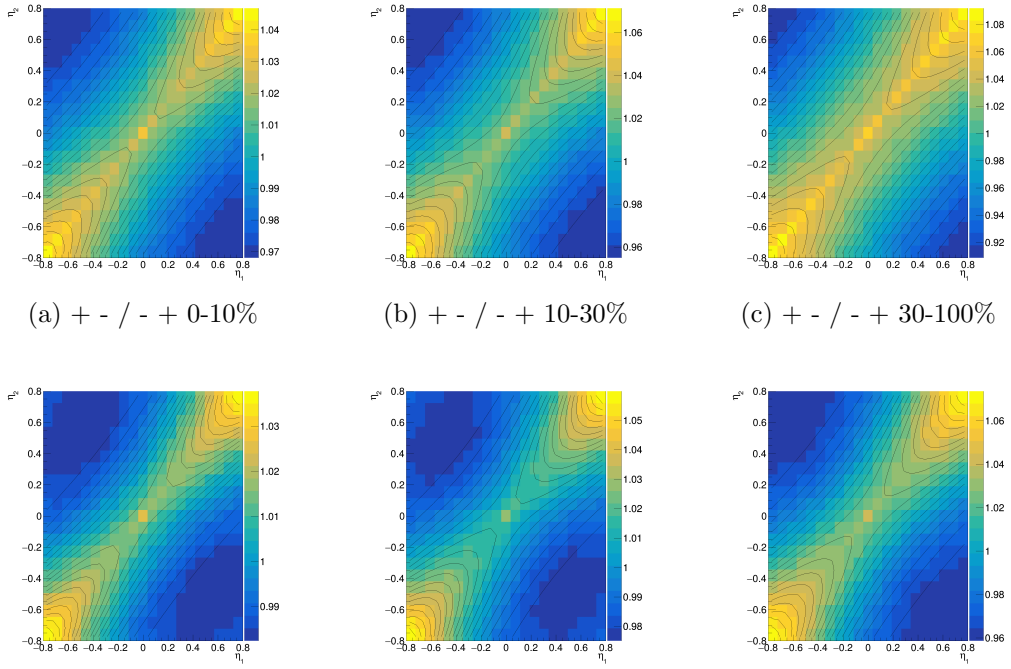

(a) + - / - + 0-10% (b) + - / - + 10-30% (c) + - / - + 30-100%

(d) + + / - - 0-10% (e) + + / - - 10-30% (f) + + / - - 30-100%

Figure 6.6: In the first row are the opposite charge combination results, while in the second row are the same charge combination results. In both lines, CL1 estimator results are shown.

6.2 The correlation function for protons and antiprotons

In this section, we present the results for proton-proton (or antiproton-antiproton) and proton-antiproton correlation functions. As we will see we have some intriguing results on the baryon-baryon correlations. However, the biggest hurdle is to get enough statistics.

6.2.1 Proton

In Figures 6.7 and 6.8 we present the results for proton and antiproton correlation functions. The first thing that we observe is that the statistics is bad compared to Figures 6.5 and 6.12. These results for the proton-antiproton correlation function was achieved by using all of the LHC18 dataset. If we use only partial data sets than the statistic will be even worse. The failure of the fitting function, as seen in Fig. 2, is the result of low statistics (this is why the fitting contour plot will not be applied to the rest of the results).

V0M

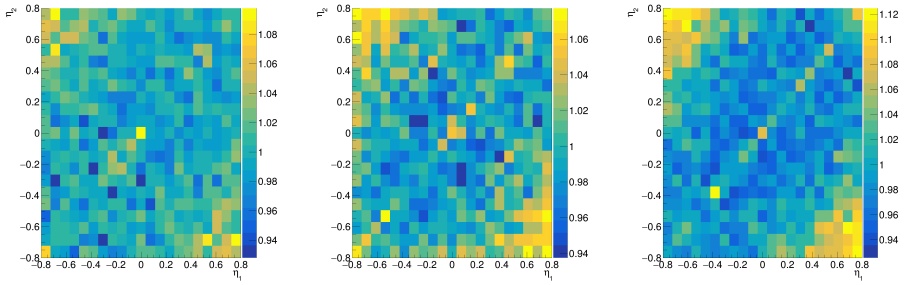

(a) ++/ - - V0M 0-10% (b) ++/ - - V0M 10-30% (c) ++/ - - V0M 30-100%

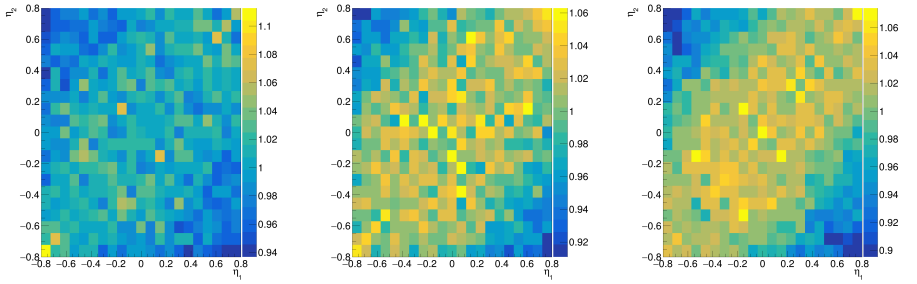

(d) +-/-+ V0M 0-10% (e) +-/-+ V0M 10-30% (f) +-/-+ V0M 30-100%

Figure 6.7: In the first row are the results for V0M same charge combination throughout all multiplicity classes, while in the second row are the results for V0M opposite charge combination and same multiplicity classes.

For the opposite charge combination in Fig. 6.7 a positive correlation is formed, where the diagonal is the most dominant. However, the correlation is more prominent in the classes of 10-30% and 30-100%. The correlation decreases and becomes

negative as the difference in pseudorapidity grows. The centre of the plot is where the correlation is the strongest. For the same charge combination in Fig. 6.7 an anti-correlation is formed. However, besides the anti-correlation, which is the most dominant, traces of positive correlation can be seen as well. The anti-correlation increases and becomes negative as the difference in pseudorapidity grows. The top left and the bottom right is where the correlation is more dominant. We can observe that as we go up in multiplicity classes more and more protons are correlated in each charge combination.

CL1

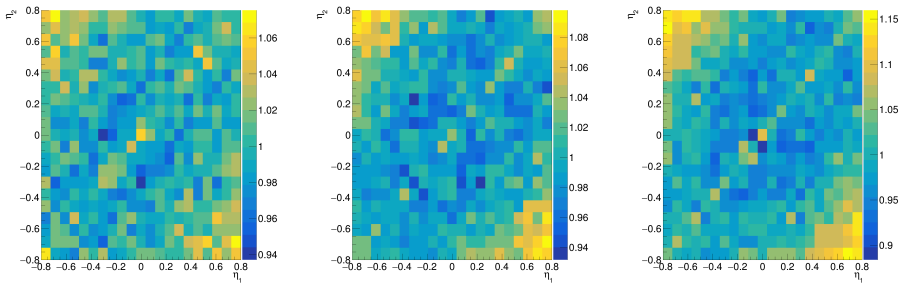

(a) ++/ - - CL1 0-10% (b) ++/ - - CL1 10-30% (c) ++/ - - CL1 30-100%

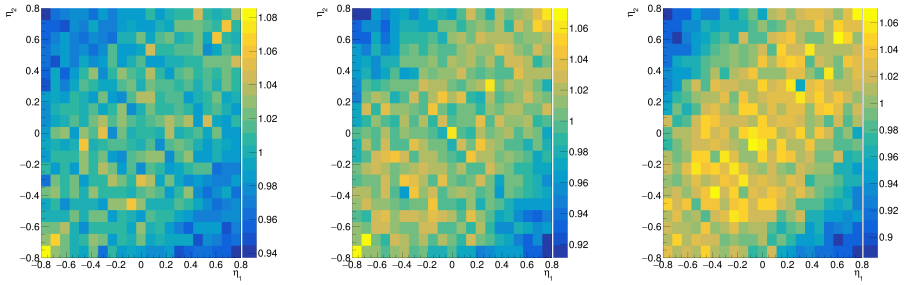

(d) +-/-+ CL1 0-10% (e) +-/-+ CL1 10-30% (f) +-/-+ CL1 30-100%

Figure 6.8: In the first row are the results for CL1 same charge combination throughout all multiplicity classes, while in the second row are the results for CL1 opposite charge combination and same multiplicity classes.

For the opposite charge combination in Fig. 6.8 a positive correlation is formed, where the diagonal is the most dominant. However, the correlation is more prominent in the classes of 10-30% and 30-100%. The correlation decreases and becomes

negative as the difference in pseudorapidity grows. The centre of the plot is where the correlation is the strongest. For the same charge combination in Fig. 6.8 an anti-correlation is formed. However, besides the anti-correlation, which is the most dominant, traces of positive correlation can be seen as well. The anti-correlation increases and becomes negative as the difference in pseudorapidity grows. The top left and the bottom right is where the correlation is more dominant. We can observe that as we go up in multiplicity classes more and more protons are correlated in each charge combination.

As we can see the LHC18 correlation function plots do not show that much better results in terms of statistics. This is something that in the future we need to enhance/consider. However, in the same charge combination, we can already see something unusual. Instead of forming a correlation, an anti-correlation is formed. This is a similar observation as in [1]. In the ALICE paper [1] same baryon number correlations have shown a suppression that is not expected in models. The baryons they investigated are the protons p and lambdas Λ. Just like in this work they have also looked at baryon-baryon and antibaryon-antibaryon as well as baryon-antibaryon combinations (protons and lambdas respectively).

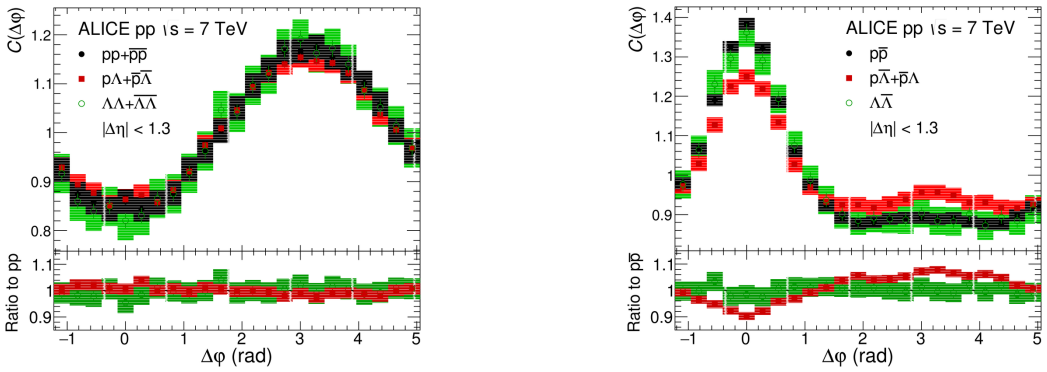

(a) Same baryon correlation

(b) Opposite baryon correlations

Figure 6.9: The suppression in the same baryon correlation function. Image from [1]

They also looked at mixed baryon correlations (proton-lambda). These baryon correlation functions showed the same suppression. In these papers [16, 17, 20] three overall possibilities were concluded. These are as follows

1. Fragmentation of hard-scattered partons

2. Resonance decays

3. Femtoscopic correlations

The fragmentation of hard-scattered partons is responsible for creating jets. However, in proton-proton collisions, we do not have any jet formulation. Resonance decays can be excluded from likely candidates for explaining the results since there is no decay that would give us two protons. Femtoscopic correlations are true for low p_T values. However, in the analysis we have used high values of p_T. None of these explain the behaviour of protons p at high p_T values. The results seem to to suggests that when a string is broken only one proton can be formed. However, we do not know how and why this process/effect happens.

6.3 The correlation function for the kaons, pions and their antiparticles

In this section, we are going to present the results for the kaons and pions. The results for these particles are in line whit what the models predict. For this analysis, both TPC and TOF were utilised.

6.3.1 Kaon

Kaons are the second lightest mesons that can detected by their stopping power and hence appear on the "Bethe-Bloch" plot. Kaons are the first branch in 3.1.

V0M

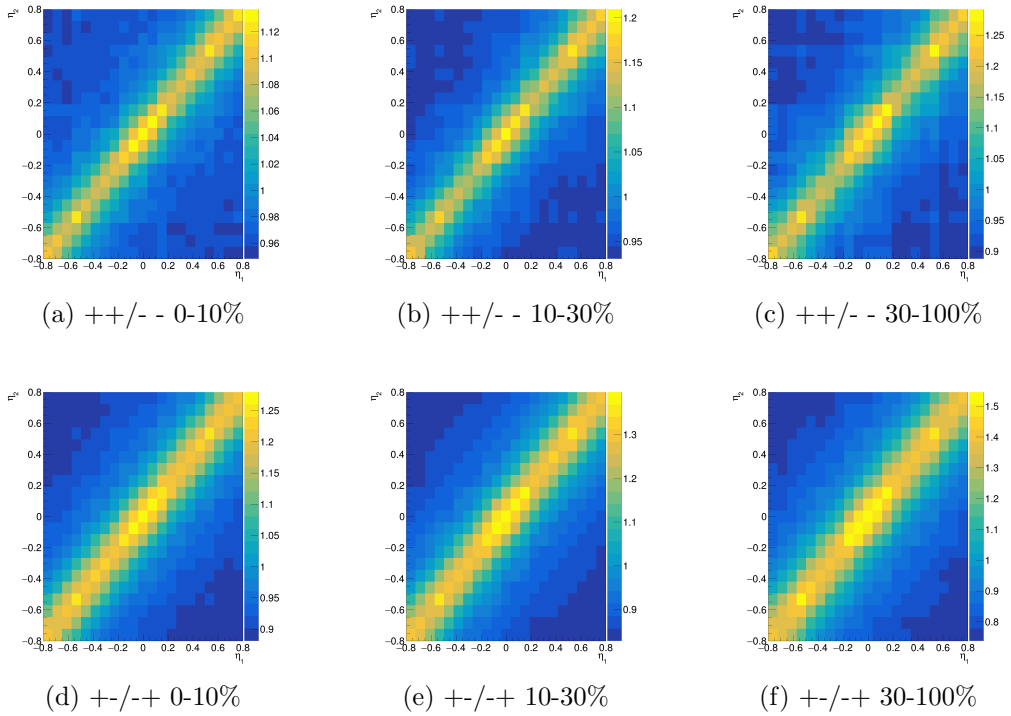

(a) ++/- - 0-10% (b) ++/- - 10-30% (c) ++/- - 30-100%

(d) +-/-+ 0-10% (e) +-/-+ 10-30% (f) +-/-+ 30-100%

Figure 6.10: V0M estimator results for same and opposite charge combination for the kaon. The analysis just like before was done for three different multiplicity classes. In the first row are the results for the same charge combination, while in the second row are the opposite charge combination.

In 6.10 we can see the V0M estimator results for kaons. In each multiplicity class and charge combination a positive correlation is formed, where the diagonal is the most dominant. The correlation decreases and becomes negative as the difference in pseudorapidity grows. Overall we can say that the opposite charge combination is more active throughout all multiplicity classes.

CL1

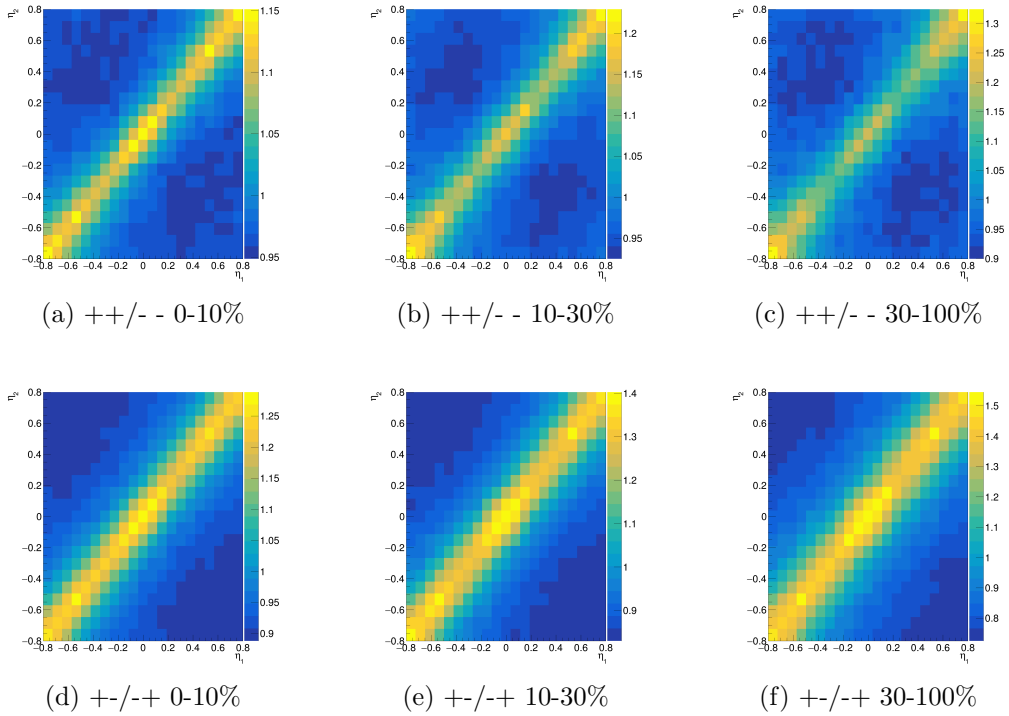

(a) ++/- - 0-10% (b) ++/- - 10-30% (c) ++/- - 30-100%

(d) +-/-+ 0-10% (e) +-/-+ 10-30% (f) +-/-+ 30-100%

Figure 6.11: CL1 estimator results for same and opposite charge combination for the kaon. The analysis just like before was done for three different multiplicity classes. In the first row are the results for the same charge combination, while in the second row are the opposite charge combination.

In 6.10 we can see the CL1 estimator's results for the kaon. In each multiplicity class and charge combination a positive correlation is formed, where the diagonal is the most dominant. The correlation decreases and becomes negative as the difference in pseudorapidity grows. However, in the first row we can observe that besides the centre, the bottom left and top right corners are dominant as well. Overall we can say that the opposite charge combination is more active throughout all multiplicity classes.

6.3.2 Pion

Pions are the lightest mesons that can detected by their stopping power and hence appear on the "Bethe-Bloch" plot. Pions are the straight line in 3.1, alongside the electrons. Pions are very much dominant in the "Bethe-Bloch" plot because, they are the strong force carriers in baryons such as protons, as well as they are decay products of heavier baryons such as lambdas.

V0M

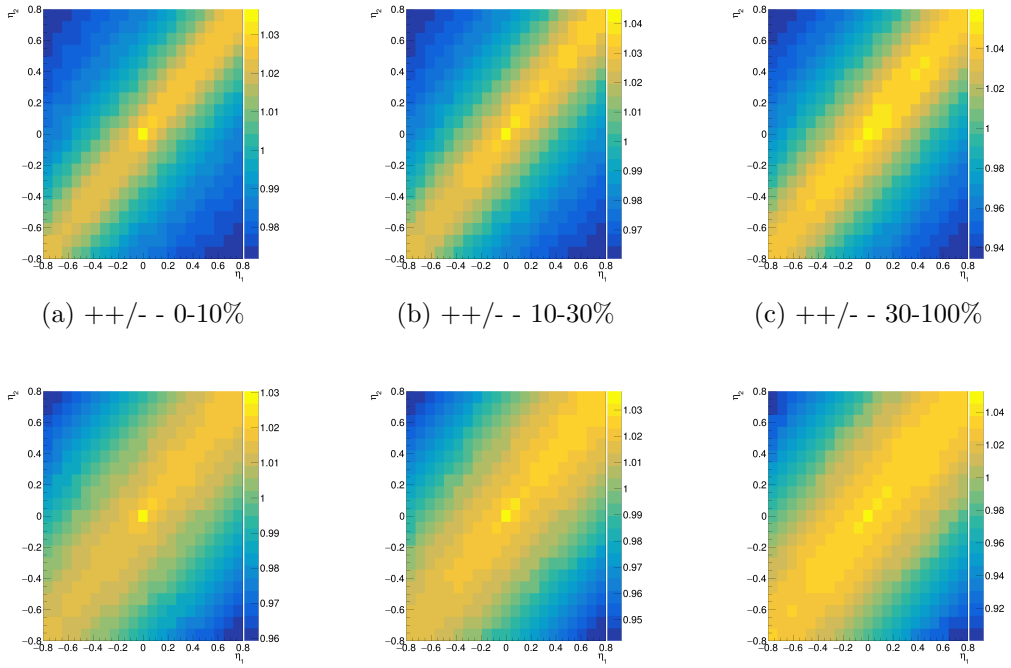

(a) ++/- - 0-10% (b) ++/- - 10-30% (c) ++/- - 30-100%

(d) +-/-+ 0-10% (e) +-/-+ 10-30% (f) +-/-+ 30-100%

Figure 6.12: V0M estimator results for same and opposite charge combination for the pion. The analysis just like before was done for three different multiplicity class. In the first row are the results for the same charge combination, while in the second row are the opposite charge combination.

In Figure 6.12 we can see the V0M estimator results for the pion. In each multiplicity class and charge combination a positive correlation is formed, where the diagonal is the most dominant. The correlation decreases and becomes negative as the difference in pseudorapidity grows. We can observe that as we go up in

multiplicity classes more and more pions are correlated in each charge combination. We also observe that the opposite charge combination correlation function is much broader than the same charge combination correlation function. Overall we can say that the opposite charge combination is more active throughout all multiplicity classes.

CL1

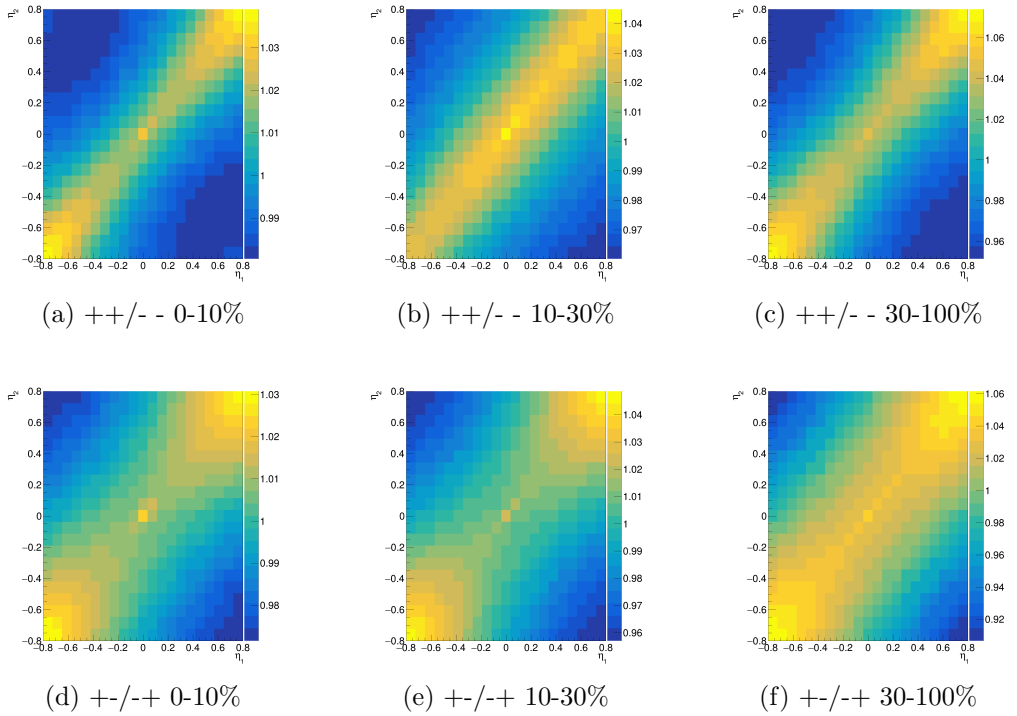

(a) ++/- - 0-10% (b) ++/- - 10-30% (c) ++/- - 30-100%

(d) +-/-+ 0-10% (e) +-/-+ 10-30% (f) +-/-+ 30-100%

Figure 6.13: CL1 estimator results for same and opposite charge combination for the pion. The analysis just like before was done for three different multiplicity classes. In the first row are the results for the same charge combination, while in the second row are the opposite charge combination.

In 6.13 we can see the CL1 estimator's results for the pion. In each multiplicity class and charge combination a positive correlation is formed, where the top right and the bottom left corners are the most dominant. The correlation increases and becomes negative as the difference in pseudorapidity grows. We can see a stronger peak in the middle of 6.13. We can observe that as we go up in multiplicity classes

more and more pions are correlated in each charge combination. We observe that the opposite charge combination correlation function is much boarder than for the same charge combination correlation function, as was the case for the V0M estimator results. Overall we can say that the opposite charge combination is more active throughout all multiplicity classes.

6.3.3 Kaon vs Pion

In this section, we are going to compare the results for pions and kaons with each other, through the previously established criteria, i.e. multiplicity estimator, multiplicity class, and charge combination.

V0M

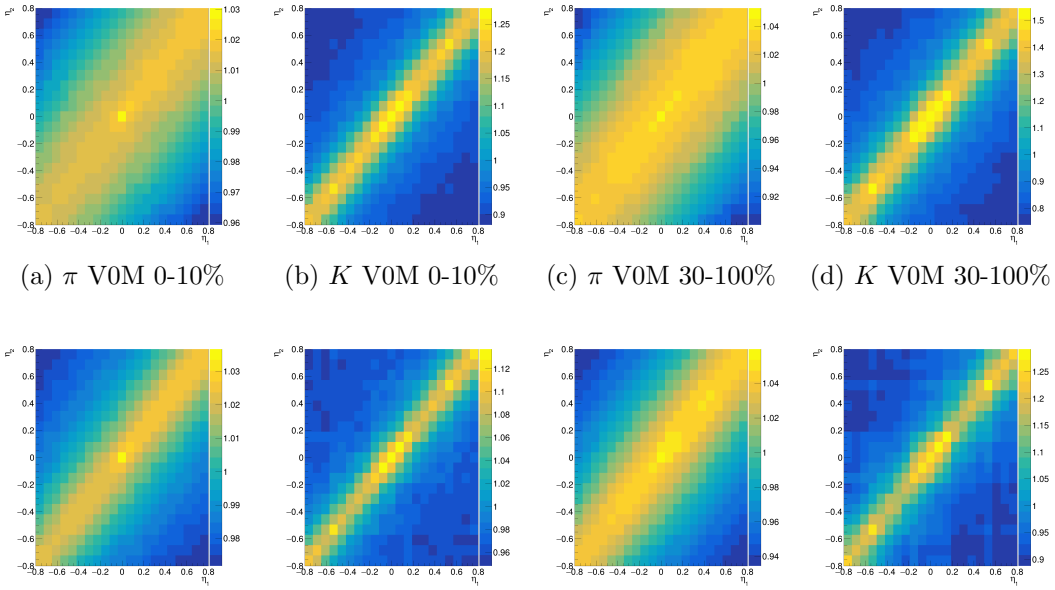

(a) π V0M 0-10% (b) K V0M 0-10% (c) π V0M 30-100% (d) K V0M 30-100%

(e) π V0M 0-10% (f) K V0M 0-10% (g) π V0M 30-100% (h) K V0M 30-100%

Figure 6.14: In the first row are the comparison between the Pions π and Kaons K for opposite charge combination, while in the second row is the comparison for same charge combination. The multiplicity classes are V0M 0-10% and V0M 30-100%.

In the V0M estimator comparison the first thing that we observe is that, the pions have better statistics than the kaons. Both types of particles form a correlation in

each multiplicity class and charge combination. For each particle case, we can see that the correlation is strongest in the centre (opposite charge combination) while for the same charge combination, the correlation is more spread out with respect to its strength. We also observe that the correlation function for the pions is much broader than the kaons. This is the result that much more pions are created (both directly and from decays) than kaons.

CL1

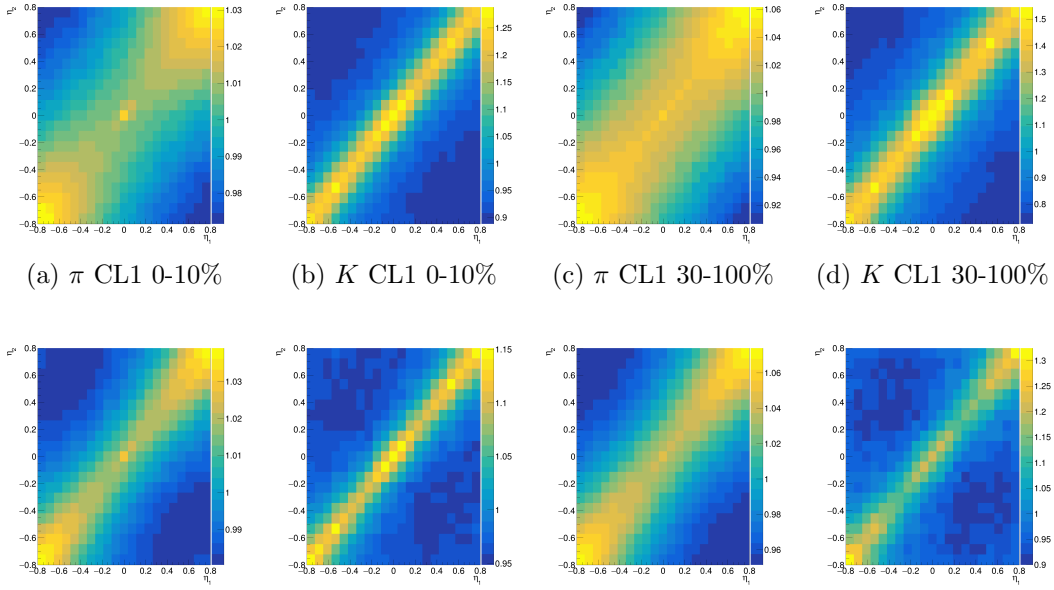

(a) π CL1 0-10% (b) K CL1 0-10% (c) π CL1 30-100% (d) K CL1 30-100%

(e) π CL1 0-10% (f) K CL1 0-10% (g) π CL1 30-100% (h) K CL1 30-100%

Figure 6.15: In the first row are the comparison between the Pions π and Kaons K for CL1 opposite charge combination, while in the second two columns are the comparison for CL1 same charge combination. The multiplicity classes are V0M 0-10% and V0M 30-100%

In the CL1 estimator comparison the first thing that we observe is that, the pions have better statistics than the kaons. Both types of particles form a correlation in each multiplicity class and charge combination. However, the most correlated regions shift towards the top right and the bottom left corners. For each particle we can observe a strong peak in the centre (especially for the kaons), however, the most correlated area for the kaon CL1 0-10% opposite charge combination is the centre. As was the case for the V0M estimator results we observe that the CL1

estimator results for the correlation function for the pions are also much broader than the kaons.

6.4 Kaon vs. Pion vs. Proton

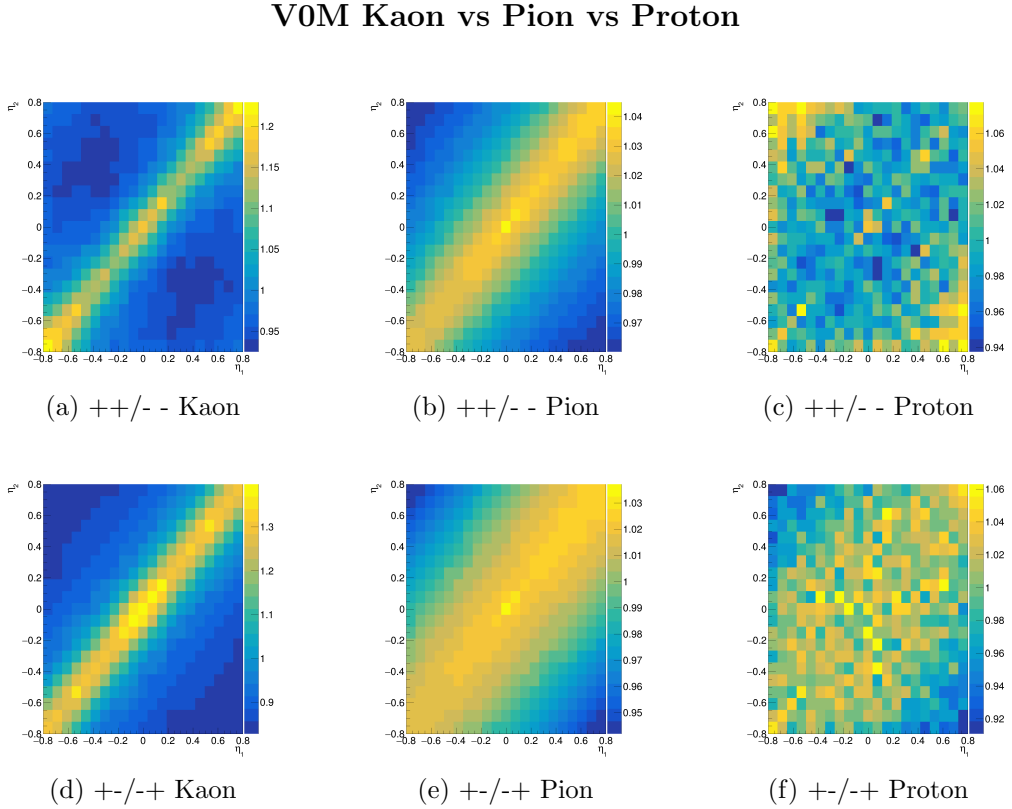

(a) ++/- - Kaon (b) ++/- - Pion (c) ++/- - Proton

(d) +-/-+ Kaon (e) +-/-+ Pion (f) +-/-+ Proton

Figure 6.16: V0M multiplicity estimator results for three types of particle: Kaon, Pion, and Proton. In the first row are the results for the same charge combination while in the second row are the opposite charge combination. In both rows the multiplicity class is 10-30%.

The first thing that we observe in 6.16 is that the statistics are not the same. The protons results have the lowest statistics, the kaons results have the second most statistics while the pions results show the most statistics. The opposite charge combination (the second row) in 6.16 shows that each type of particle formed a correlation. The centre of these plots is where the correlation is strongest. The

same charge combination (the first row) in 6.16, tells a different story. While the pions and kaons form a positive correlation, the protons form an anti-correlation. However, a strong(ish) peak can be observed in the middle for each of them.

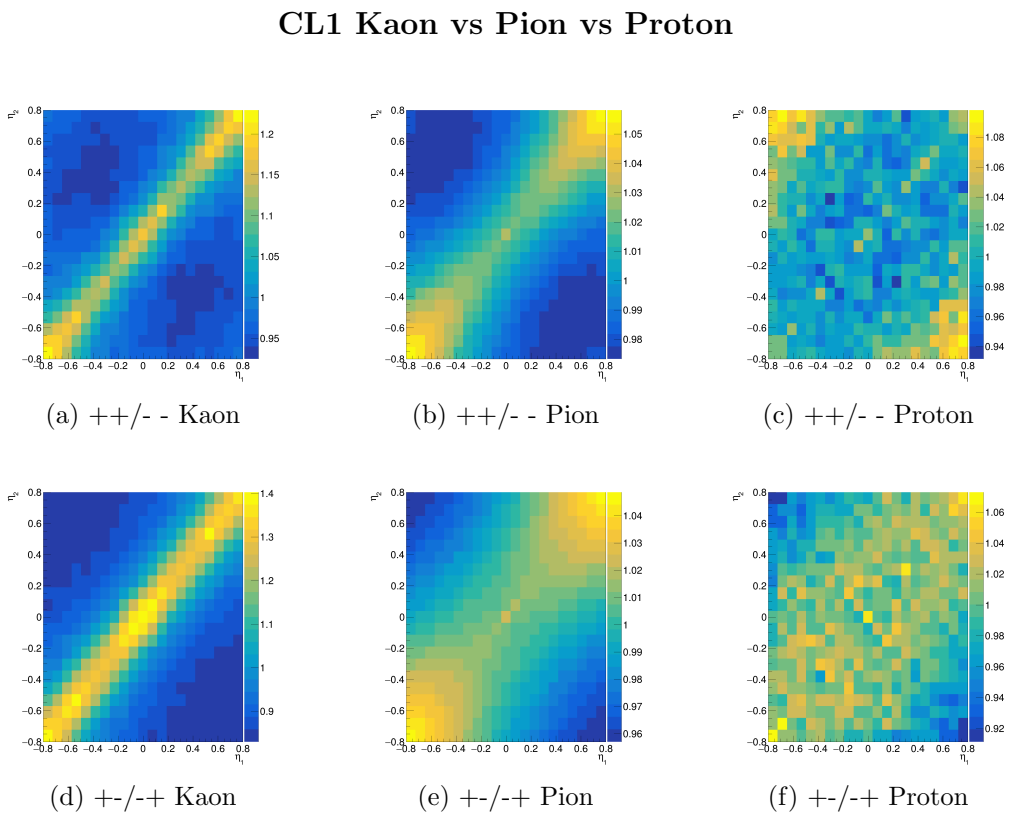

(a) ++/- - Kaon (b) ++/- - Pion (c) ++/- - Proton

(d) +-/-+ Kaon (e) +-/-+ Pion (f) +-/-+ Proton

Figure 6.17: CL1 multiplicity estimator results for three types of particle: Kaon K, Pion π, and Proton p. In the first row are the results for the same charge combination while in the second row are the opposite charge combination. In both rows the multiplicity class is 10-30%.

The first thing that we observe in 6.16 is that the statistics are not the same. The protons results have the lowest statistics, the kaons results have the second most statistics while the pions results show the most statistics. The opposite charge combination (the second row) in 6.16 shows that each type of particle formed a positive correlation. The top right and bottom left corners are where the correlation is strongest, although the correlation for the kaons is more evenly spread out. The same charge combination (the first row) in 6.16, tells a similar

story. While the pions and kaons form a correlation, the proton forms an anti-correlation. However, a strong(ish) peak can be observed in the middle for each of them. The kaons correlation is more evenly spread out in the case of the CL1 estimator as well.

Chapter 7

Outlook

In this thesis, the analysis only included the proton and two mesons, namely the kaons K and pions π. As we have seen in the previous section the two mesons show a correlation in each multiplicity class and charge combination while the proton only shows this correlation for the opposite charge combination. For the same charge combination, the proton shows an anti-correlation. This anti-correlation was observed in [1], and it was the primary motivation for this thesis. What else could be done? Just as in [1] the analyses could be expanded for lambda particles and as well a mixed baryon (proton-lambda) analysis could be done as well. Perhaps the analysis could be even extended for the xi particles as well.

Further improvements that could be done for this analysis include Monte Carlo simulations and to look at even more data. The Monte Carlo simulations would/could correct the pseudorapidity, which therefore would enhance the efficiency. As we have seen on the proton (6.7, 6.8, 6.16 and 6.17) the statistics are not good even though the full LHC18 data set was used. To improve this we could look at LHC17 (together with the LHC18) and of course, these results could be enhanced by future runs of the LHC.

Chapter 8

Conclusion

This thesis' goal was to measure baryon correlations in proton-proton collisions at $\sqrt{s} = 13$ TeV. In this thesis, we studied multiplicity correlations in pseudorapidity for different charge combinations (++/- - and +-/-+) as well as for the forward-backwards region of ALICE, two multiplicity estimators were used namely the CL1 and the V0M. For these estimators, the following multiplicity classes were attributed: 0-10%, 10-30% and 30-100%.

In this thesis, PID was also carried out, where we have identified two mesons, namely the pions π and the kaons K, and a baryon which is the proton p. The correlation function for the mesons shows a correlation for both multiplicity estimators. On the other hand, we have seen that there is a suppression in the same baryon correlation function while there is no suppression for the opposite correlation function.

Appendix

In this appendix all the results regarding the PID will be presented. For discussion of these results see Chapter 6.

Proton correlation function

In Fig. 1 shows all of the proton-antiproton correlation function results *without* the fitting function 5.8, 5.9 and 5.10 for a given multiplicity estimator (V0M and CL1) and charge combination (same for + + / - - and opposite for + - / - +). The multiplicity classes (0-10%, 10-30% and 30-100%) are also shown under the given plot.

In Fig. 2 shows all of the proton-antiproton correlation function results *with* the fitting function 5.8, 5.9 and 5.10. The layout of Fig. 2 is the same as in Fig. 1.

V0M and CL1 for protons (unfitted)

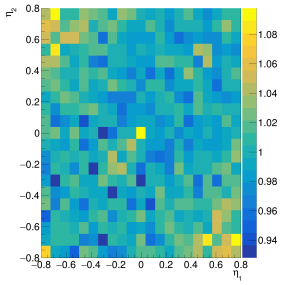

(a) + + / - - 0-10%

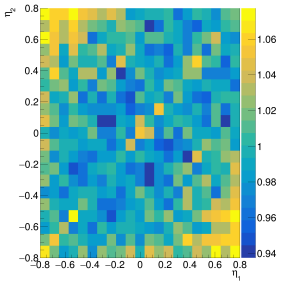

(b) + + / - - 10-30%

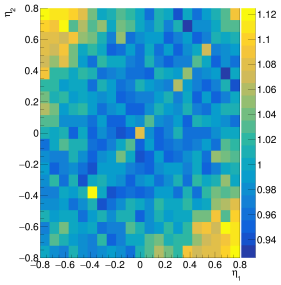

(c) + + / - - 30-100%

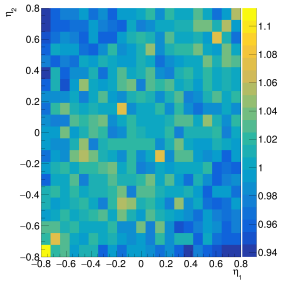

(d) + - / - + 0-10%

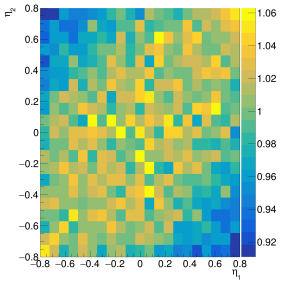

(e) + - / - + 10-30%

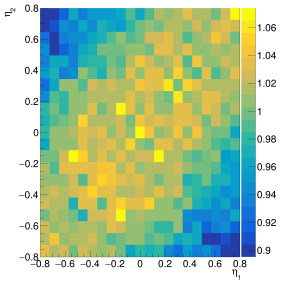

(f) + - / - + 30-100%

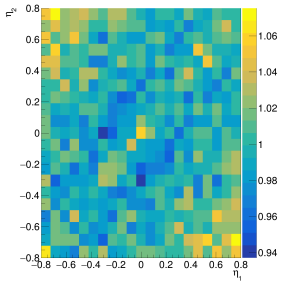

(g) + + / - - 0-10%

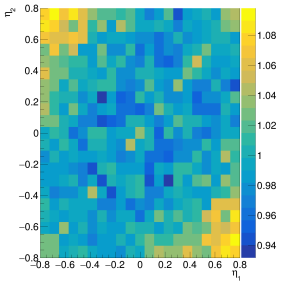

(h) + + / - - 10-30%

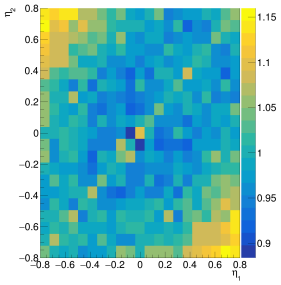

(i) + + / - - 30-100%

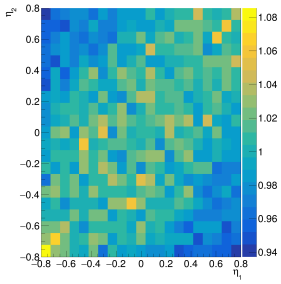

(j) + - / - + 0-10%

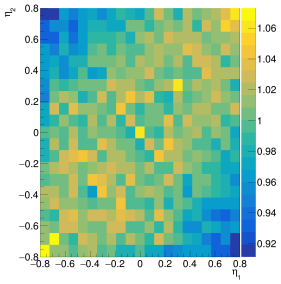

(k) + - / - + 10-30%

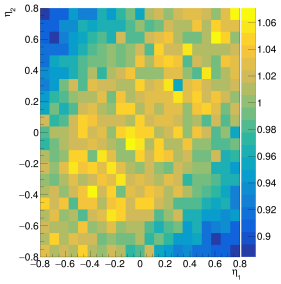

(l) + - / - + 30-100%

Figure 1: From (a)-(f) the V0M results are shown, while from (g)-(l) the CL1 results are shown for protons p. Under each plot, the charge combination and multiplicity class is shown.

V0M and CL1 for protons (fitted)

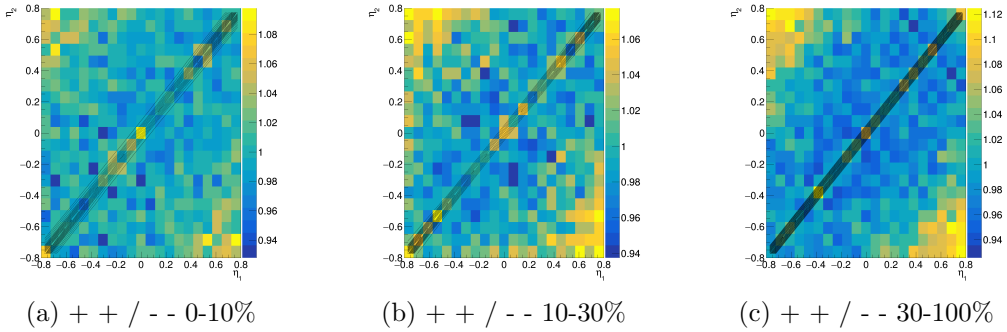

(a) + + / - - 0-10% (b) + + / - - 10-30% (c) + + / - - 30-100%

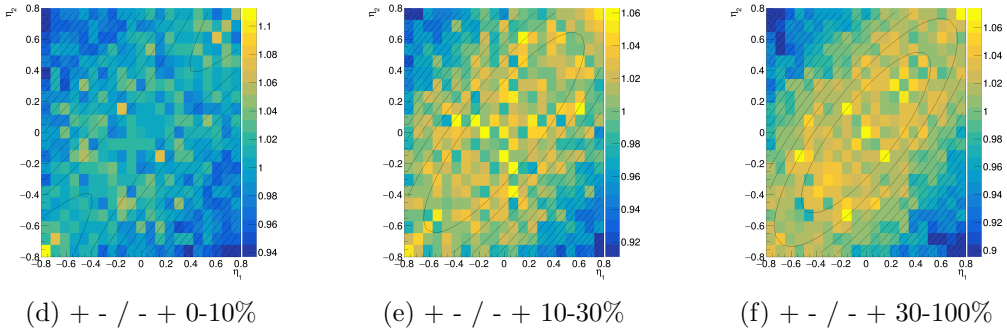

(d) + - / - + 0-10% (e) + - / - + 10-30% (f) + - / - + 30-100%

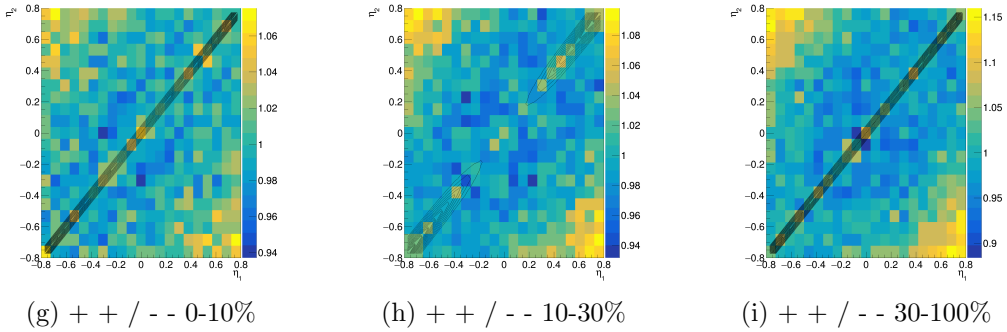

(g) + + / - - 0-10% (h) + + / - - 10-30% (i) + + / - - 30-100%

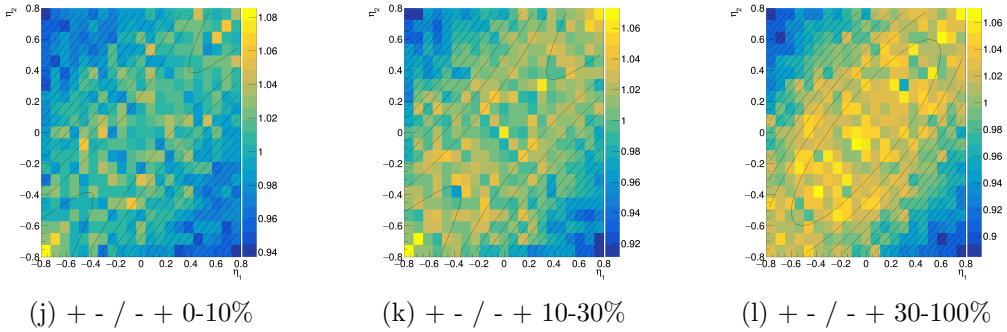

(j) + - / - + 0-10% (k) + - / - + 10-30% (l) + - / - + 30-100%

Figure 2: From (a)-(f) the V0M results are shown, while from (g)-(l) the CL1 results are shown for protons p. Under each plot, the charge combination and multiplicity class is shown.

Kaon correlation function

In Fig. 3 shows all of the kaon-antikaon correlation function results *without* the fitting function 5.8, 5.9 and 5.10 for a given multiplicity estimator (V0M and CL1) and charge combination (same for + + / - - and opposite for + - / - +). The multiplicity classes (0-10%, 10-30% and 30-100%) are also shown under the given plot.

In Fig. 4 shows all of the kaon-antikaon correlation function results *with* the fitting function 5.8, 5.9 and 5.10. The layout of Fig. 4 is the same as in Fig. 3.

V0M and CL1 for kaons (unfitted)

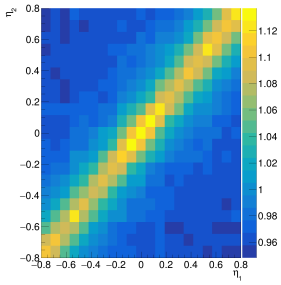

(a) + + / - - 0-10%

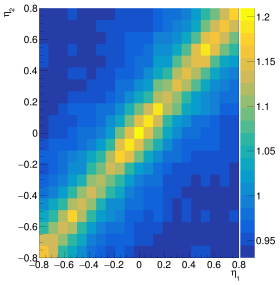

(b) + + / - - 10-30%

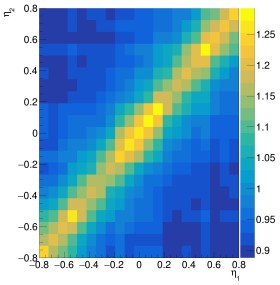

(c) + + / - - 30-100%

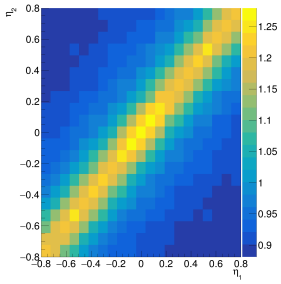

(d) + - / - + 0-10%

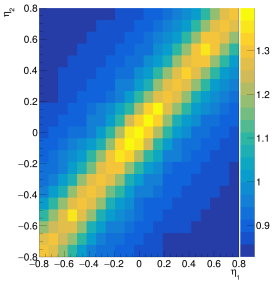

(e) + - / - + 10-30%

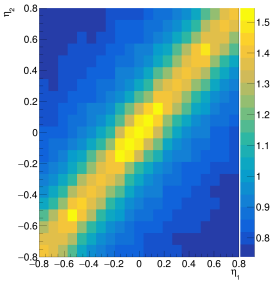

(f) + - / - + 30-100%

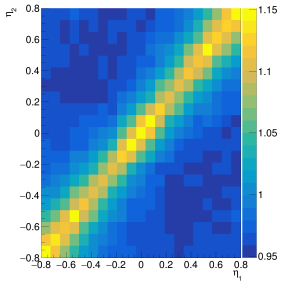

(g) + + / - - 0-10%

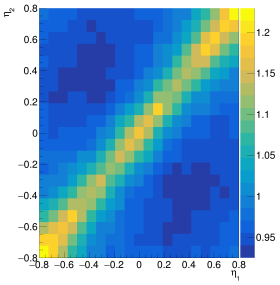

(h) + + / - - 10-30%

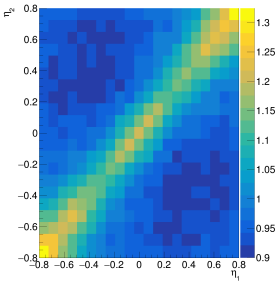

(i) + + / - - 30-100%

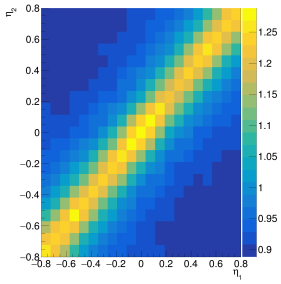

(j) + - / - + 0-10%

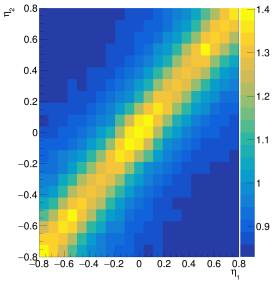

(k) + - / - + 10-30%

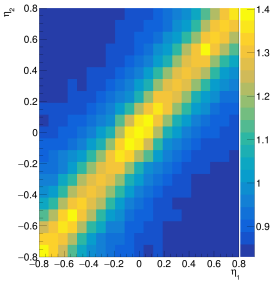

(l) + - / - + 30-100%

Figure 3: From (a)-(f) the V0M results are shown, while from (g)-(l) the CL1 results are shown for kaons K. Under each plot, the charge combination and multiplicity class is shown.

V0M and CL1 for kaons (fitted)

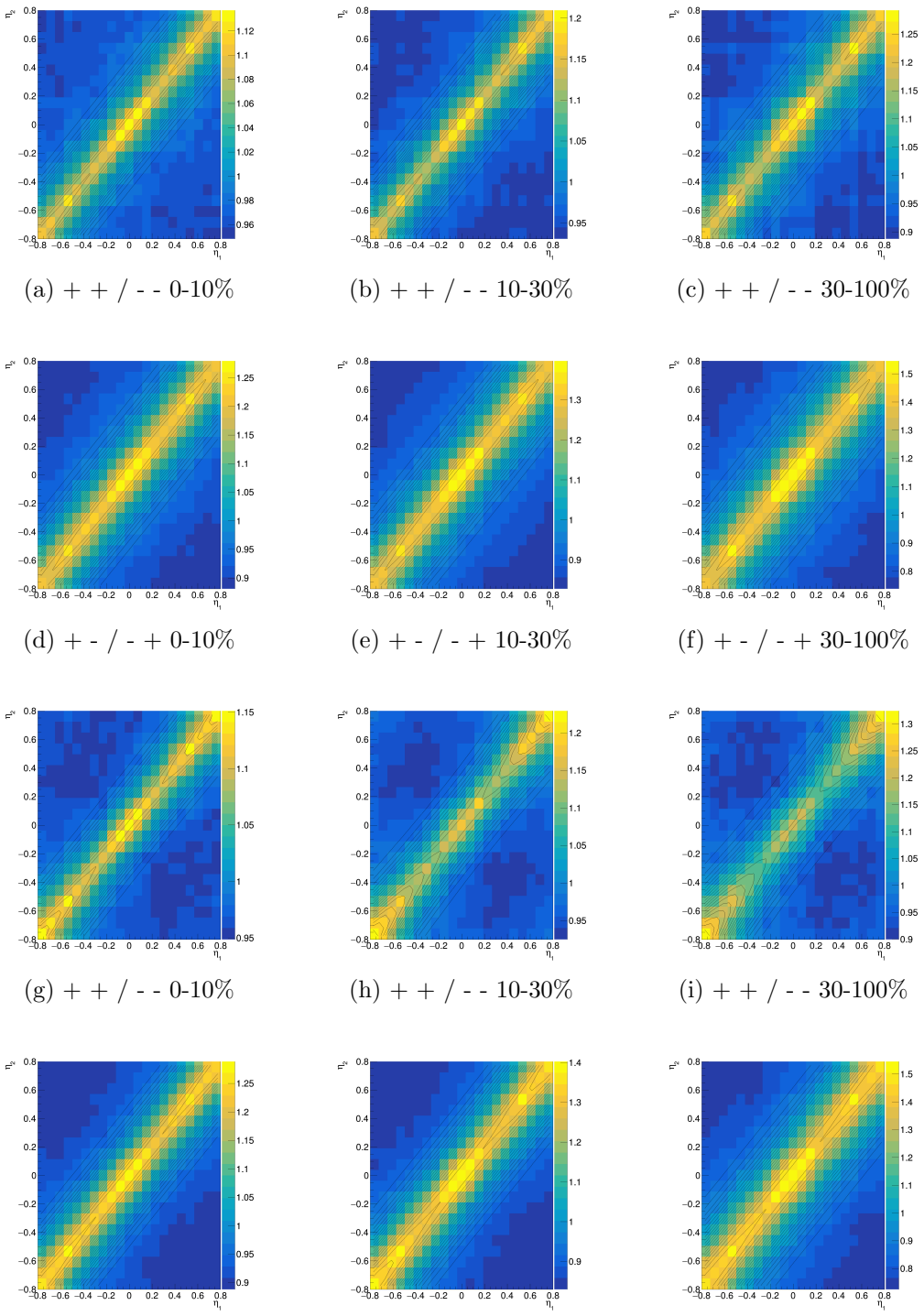

(a) + + / - - 0-10% (b) + + / - - 10-30% (c) + + / - - 30-100%

(d) + - / - + 0-10% (e) + - / - + 10-30% (f) + - / - + 30-100%

(g) + + / - - 0-10% (h) + + / - - 10-30% (i) + + / - - 30-100%

(j) + - / - + 0-10% (k) + - / - + 10-30% (l) + - / - + 30-100%

Figure 4: From (a)-(f) the V0M results are shown, while from (g)-(l) the CL1 results are shown for kaons K. Under each plot, the charge combination and multiplicity class is shown.

Pion correlation function

In Fig. 5 shows all of the pion-antipion correlation function results *without* the fitting function 5.8, 5.9 and 5.10 for a given multiplicity estimator (V0M and CL1) and charge combination (same for + + / - - and opposite for + - / - +). The multiplicity classes (0-10%, 10-30% and 30-100%) are also shown under the given plot.

In Fig. 6 shows all of the pion-antipion correlation function results *with* the fitting function 5.8, 5.9 and 5.10. The layout of Fig. 6 is the same as in Fig. 5.

V0M and CL1 for pions (unfitted)

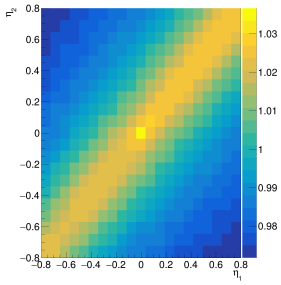

(a) + + / - - 0-10%

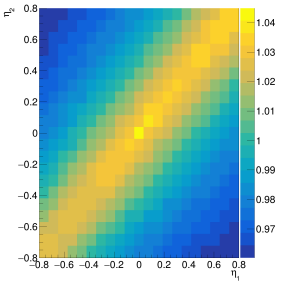

(b) + + / - - 10-30%

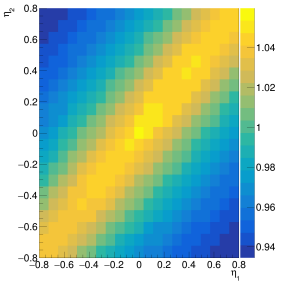

(c) + + / - - 30-100%

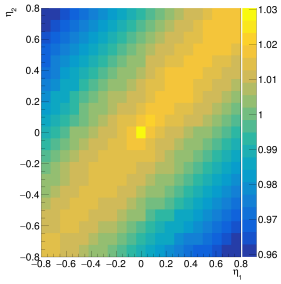

(d) + - / - + 0-10%

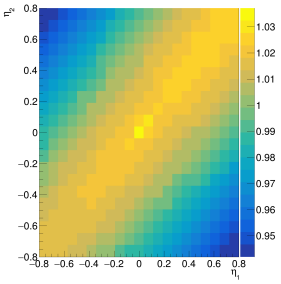

(e) + - / - + 10-30%

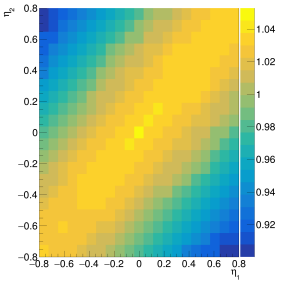

(f) + - / - + 30-100%

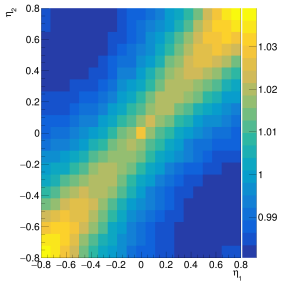

(g) + + / - - 0-10%

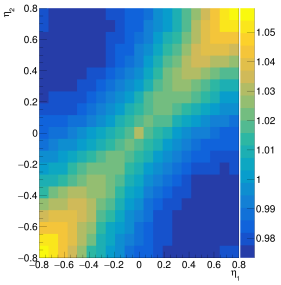

(h) + + / - - 10-30%

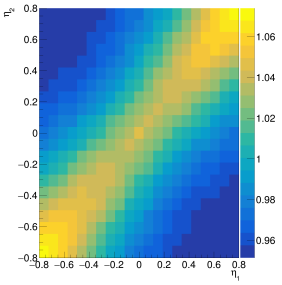

(i) + + / - - 30-100%

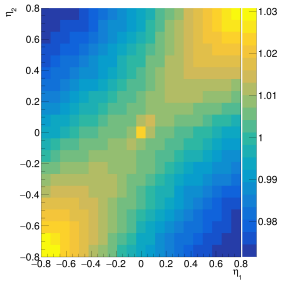

(j) + - / - + 0-10%

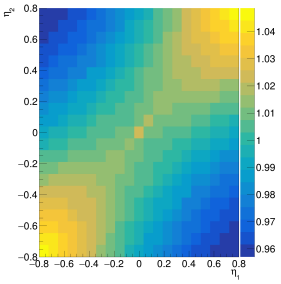

(k) + - / - + 10-30%

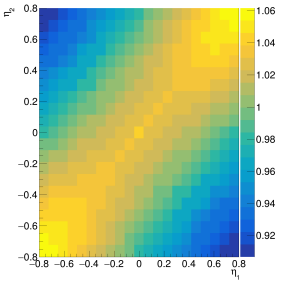

(l) + - / - + 30-100%

Figure 5: From (a)-(f) the V0M results are shown, while from (g)-(l) the CL1 results are shown for pions π. Under each plot, the charge combination and multiplicity class is shown.

V0M and CL1 for pions (fitted)

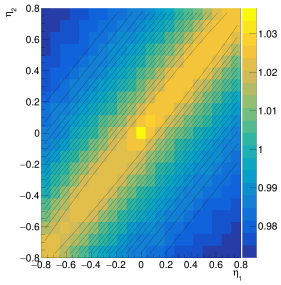

(a) + + / - - 0-10%

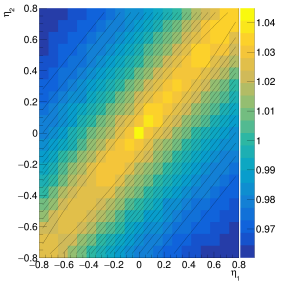

(b) + + / - - 10-30%

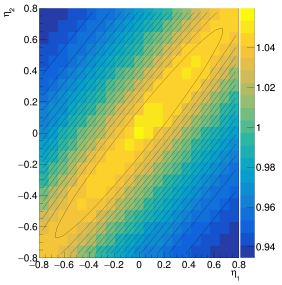

(c) + + / - - 30-100%

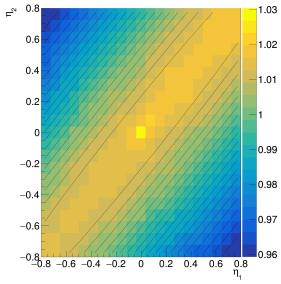

(d) + - / - + 0-10%

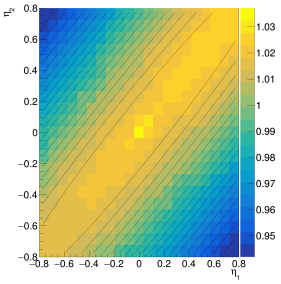

(e) + - / - + 10-30%

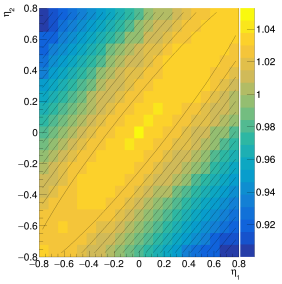

(f) + - / - + 30-100%

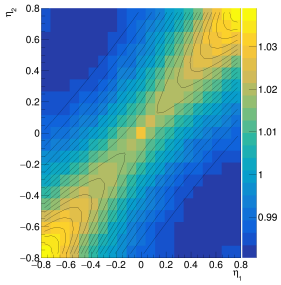

(g) + + / - - 0-10%

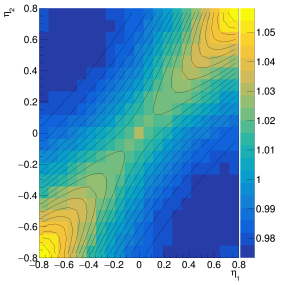

(h) + + / - - 10-30%

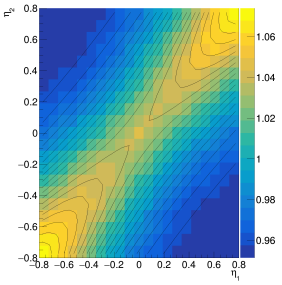

(i) + + / - - 30-100%

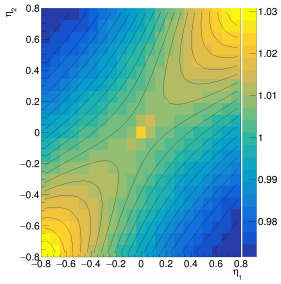

(j) + - / - + 0-10%

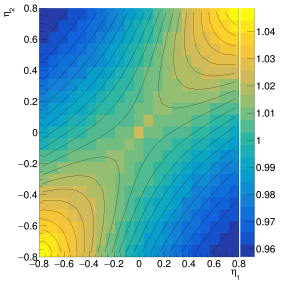

(k) + - / - + 10-30%

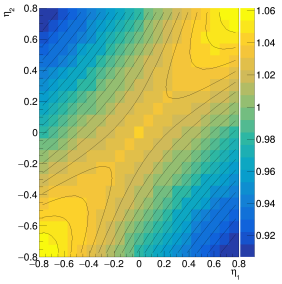

(l) + - / - + 30-100%

Figure 6: From (a)-(f) the V0M results are shown, while from (g)-(l) the CL1 results are shown for pions π. Under each plot, the charge combination and multiplicity class is shown.

References

[1] Insight into particle production mechanisms via angular correlations of identified particles in pp collisions at $\sqrt{s}$=7 TeV ; arXiv:1612.08975 (2016)

[2] M. Peskin, D. Schroeder: 'Introduction to quantum field theory' ; CRC Press (2018)

[3] M. Schwartz: 'Quantum Field Theory and the Standard Model' ; Cambridge University Press (2014)

[4] W. Greiner, J. Reinhardt: 'Quantum Electrodynamics' ; Fourth edition, Springer (2009)

[5] W. Greiner, B. Müller: 'Gauge Theory of Weak Interactions' ; Fourth edition, Springer (2009)

[6] M. Connors, C. Nattrass, R. Reed, and S. Salur: 'Review of Jet measurements in Heavy Ion Collisons' ; Rev. Mod. Phys. 90, 025005 (2018)

[7] The ALICE homepage
`https://www.home.cern/science/experiments/alice`

[8] G. Aad: 'Observation of a Centrality-Dependent Dijet Asymmetry in Lead-Lead Collisions at $\sqrt{s_{NN}}$= 2.76 TeV with the ATLAS Detector at the LHC' ; Phys.Rev.Lett. 105:252303, (2010)

[9] ATLAS collaboration: 'Measurements of the Nuclear Modification Factor for Jets in Pb+Pb Collisions at $\sqrt{s_{NN}}$=2.76 TeV with the ATLAS Detector' ; Phys. Rev. Lett. 114 072302, (2015)

[10] U. A. Wiedemann: 'Jet Quenching in Heavy Ion Collisions' ; arXiv:0908.2306 [hep-ph].

[11] A. Majumder and M. Van Leeuwen: 'The theory and phenomenology of perturbative QCD based jet quenching' ; Prog.Part.Nucl.Phys 66 (2011) 41-92

[12] Wikipedia: 'Pseudorapidity'
https://en.wikipedia.org/wiki/Pseudorapidity

[13] Quantum Diaries: 'The Standard Model: a beautiful but flawed theory'
http://www.quantumdiaries.org/2014/03/14/
the-standard-model-a-beautiful-but-flawed-theory/

[14] L. Lönnbald: 'Lund strings in dense environments'
https://indico.cern.ch/event/625304/contributions/2771438/
attachments/1573428/2483574/MPI17b.pdf

[15] C. Bierlich, S. Chakraborty, N. Desai and others: ' A comprehensive guide to the physics and usage of PYTHIA 8.3' ; SciPost Phys. Codeb. , (2022)

[16] ALICE Collaboration: 'Femtoscopy of pp collisions at $\sqrt{s} = 0.9$ and 7 TeV at the LHC with two-pion Bose-Einstein correlations' ; Phys.Rev. D84 (2011) 112004

[17] STAR Collaboration: 'Measurement of Interaction between Antiprotons' ; Nature 527 (2015) 345–348

[18] M. Delmastro: 'Experimental particle physics I.'
https://indico.cern.ch/event/294651/contributions/671927/
attachments/552039/760667/Delmastro_ESIPAP2014_1.pdf

[19] T. Felser, M. Trenti, L. Sestini, A. Gianelle, D. Zuliani, D. Lucchesi, S. Montangero: 'Quantum-inspired Machine Learning on high-energy physics data' npj Quantum Inf 7, 111 (2021)

[20] R. Engel, J. Ranft, and S. Roesler: 'Hard diffraction in hadron-hadron interactions and in photoproduction' ; Phys.Rev. D52 (1995) 1459–1468

[21] A. Koppers: Forward-Backward Multiplicity Correlations for Proton-Proton Collisions with ALICE at LHC-CERN (2022) http://lup.lub.lu.se/
student-papers/record/9081656

[22] Relativistic Heavy-Ion Collider https://www.bnl.gov/rhic/

[23] Brookhaven National Laboratory https://www.bnl.gov/world/

[24] European Organisation for Nuclear Research https://home.cern/

[25] The Large Hadron Collider https://home.cern/science/accelerators/large-hadron-collider

[26] The Large Hadron Collider beauty https://lhcb.web.cern.ch/

[27] The Compact Muon Solenoid https://cms.cern/

[28] A Large Ion Collider Experiment https://alice-collaboration.web.cern.ch/

[29] A Torodial LHC Apparatus https://atlas.cern/